


CDKL5 Deficiency Augments Inhibitory Input into the Dentate Gyrus That Can Be Reversed by Deep Brain Stimulation

 Shuang Hao,^{1,2*} Qi Wang,^{1,2*} Bin Tang,^{1,2} Zhenyu Wu,^{1,2} Tingting Yang,^{1,2,3} and Jianrong Tang^{1,2}

¹Jan and Dan Duncan Neurological Research Institute, Texas Children's Hospital, Houston, Texas 77030, ²Department of Pediatrics, Baylor College of Medicine, Houston, Texas 77030, and ³Department of Neurology, People's Hospital of Guizhou Province, Guiyang, 560000, China

Cognitive impairment is a core feature of cyclin-dependent kinase-like 5 (CDKL5) deficiency, a neurodevelopmental disorder characterized by early epileptic seizures, intellectual disability, and autistic behaviors. Although loss of CDKL5 affects a number of molecular pathways, very little has been discovered about the physiological effects of these changes on the neural circuitry. We therefore studied synaptic plasticity and local circuit activity in the dentate gyrus of both *Cdkl5*^{-ly} and *Cdkl5*^{+/-} mutant mice. We found that CDKL5 haploinsufficiency in both male and female mice impairs hippocampus-dependent learning and memory in multiple tasks. *In vivo*, loss of CDKL5 reduced LTP of the perforant path to the dentate gyrus and augmented feedforward inhibition in this pathway; *ex vivo* experiments confirmed that excitatory/inhibitory input into the dentate gyrus is skewed toward inhibition. Injecting the GABAergic antagonist gabazine into the dentate improved contextual fear memory in *Cdkl5*^{-ly} mice. Finally, chronic fornical deep brain stimulation rescued hippocampal memory deficits, restored synaptic plasticity, and relieved feedforward inhibition in *Cdkl5*^{+/-} mice. These results indicate that CDKL5 is important for maintaining proper dentate excitatory/inhibitory balance, with consequences for hippocampal memory.

Key words: CDKL5; deep brain stimulation; dentate gyrus; feedforward inhibition; memory; MOPP cells

Significance Statement

Cognitive impairment is a core feature of cyclin-dependent kinase-like 5 (CDKL5) deficiency disorder. Although CDKL5 deficiency has been found to affect a number of molecular pathways, little is known about its physiological effects on the neural circuitry. We find that CDKL5 loss reduces hippocampal synaptic plasticity and augments feedforward inhibition in the perforant path to the dentate gyrus *in vivo* in *Cdkl5* mutant mice. Chronic fornical deep brain stimulation rescued hippocampal memory deficits, restored synaptic plasticity, and relieved feedforward inhibition in *Cdkl5*^{+/-} mice, as it had previously done with Rett syndrome mice, suggesting that such stimulation may be useful for other neurodevelopmental disorders.

Introduction

CDKL5 deficiency disorder (CDD) is a neurodevelopmental disease caused by mutation of the X-linked gene cyclin-dependent kinase-like 5 (*CDKL5*). CDD is characterized by severe intellectual disability, gross motor impairment, early-onset epilepsy, and autistic features (Kalscheuer et al., 2003; Weaving et al., 2004). Mouse models of CDD faithfully recapitulate the cognitive deficits and other characteristics of this condition (Wang et al., 2012; Fuchs et al., 2015; Okuda et al., 2018). Global KO/knock-in mutation of *CDKL5* or conditional CDKL5 loss in forebrain excitatory neurons impairs hippocampus-dependent memory in mice (Wang et al., 2012; Trazzi et al., 2016; Tang et al., 2017; Okuda et al., 2018; Yennawar et al., 2019), but it is not known how CDKL5 loss affects the functioning of the hippocampal circuit.

Only a few studies have addressed the influence of CDKL5 on synaptic function in the CA1 region of the hippocampus. Deleting CDKL5 from forebrain glutamatergic or GABAergic

Received May 13, 2021; revised July 16, 2021; accepted Aug. 16, 2021.

Author contributions: Q.W. and J.T. designed research; S.H., Q.W., B.T., Z.W., T.Y., and J.T. performed research; S.H., Q.W., and J.T. analyzed data; S.H., Q.W., and J.T. wrote the paper.

This work was supported in part by the National Institute of Neurological Disorders and Stroke R01NS100738 to J.T.; the LouLou Foundation to J.T.; the Eunice Kennedy Shriver National Institute of Child Health and Human Development (U54HD083092, P50HD103555 to Baylor College of Medicine Intellectual and Developmental Disabilities Research Center, Neuroconnectivity Core, Circuit Modulation Core, Neurovisualization Core); the *In Vivo* Neurophysiology Core of Jan and Dan Duncan Neurological Research Institute at Texas Children's Hospital; the Chao Family Foundation; and the Cockrell Family Foundation. We thank Dr. Huda Y. Zoghbi, Dr. Jin Xu, Vicky Brandt, and Emily W. Schaffer for critical reading of the manuscript.

S. Hao's present address: College of Life and Health Sciences, Northeastern University, Shenyang 110169, China.

*S.H. and Q.W. contributed equally to this work.

The authors declare no competing financial interests.

Correspondence should be addressed to Jianrong Tang at jtang1@bcm.edu.

<https://doi.org/10.1523/JNEUROSCI.1010-21.2021>

Copyright © 2021 the authors

neurons affects synaptic transmission and the overall excitatory/inhibitory (E/I) balance in the CA1 pyramidal neurons (Tang et al., 2017, 2019). Yet in slice preparations, global CDKL5 loss enhances LTP of synaptic transmission in the Shaffer collateral to CA1 pathway (Okuda et al., 2017; Yennawar et al., 2019). Another key component of the hippocampal formation for learning and memory is the dentate gyrus (DG) (Liu et al., 2012; Hainmueller and Bartos, 2020). The DG is crucial for gating/processing contextual, place, and spatial information from the entorhinal cortex to the hippocampus (Hargreaves et al., 2005). It is responsible for important cognitive functions, such as pattern separation (Leutgeb et al., 2007; McHugh et al., 2007), pattern completion (Nakashiba et al., 2012), and spatial and working memory (Lee and Jung, 2017; Sasaki et al., 2018). Because synaptic transmission and plasticity of the perforant path (PP) to the DG play an important role in hippocampus-dependent learning and memory (I. W. Jones et al., 2001; McHugh et al., 2007), we hypothesized that loss of CDKL5 causes memory deficits by specifically impairing this pathway.

We therefore set out to delineate the precise impairments of the hippocampal circuit in a mouse model of CDD. We used behavioral, *in vivo* and *ex vivo* approaches to discover that increased feedforward inhibition, mediated by molecular layer perforant pathway (MOPP) cells (Li et al., 2013), is the chief neural circuit mechanism that underlies memory dysfunction. Given that deep brain stimulation (DBS) effectively modulates neural circuit activity (Bouthour et al., 2019; Lozano et al., 2019), we also tested whether fornical DBS can relieve the feedforward inhibition and rescue hippocampal memory and synaptic plasticity deficits in *Cdkl5* mutant mice.

Materials and Methods

Animals

The CDKL5 mouse line was obtained from The Jackson Laboratory and maintained on the C57BL/6J background (B6.129(FVB)-*Cdkl5*^{tm1.1Joez/J}, stock #021967) (Wang et al., 2012). Adult male *Cdkl5*^{-/-} (4 months of age) and female *Cdkl5*^{+/-} (4 or 6 months of age) and age-/gender-matched WT littermates (*Cdkl5*^{+/-} and *Cdkl5*^{+/+}) were housed in a 14 h light/10 h dark cycle (light on at 6:00 A.M.) with standard mouse chow and water *ad libitum* in our on-site American Association for Laboratory Animal Science-accredited facility. The longer light cycle was used to mimic the Spring and Summer daylight hours to help with mouse breeding. Mice were group-housed up to 5 per cage without/ before surgery but housed individually with nesting material in the cage after surgery in a room maintained at 22°C. All the experimental procedures and tests were conducted during the light phase. Behavioral, electrophysiological, and immunohistochemical assays were performed and analyzed blind to genotypes and/or treatments. All research and animal care procedures were approved by the Baylor College of Medicine Institutional Animal Care and Use Committee.

Behavioral assays

All behavioral studies were conducted blinded to genotype. Mice were allowed to habituate to the testing room for at least 30 min before any test, and testing was performed around the same time of day. Open field test was conducted 1 week before fear conditioning or water maze tasks. The light intensity of 150 lux and the background white noise at 60 dB were consistently presented during the habituation and throughout the testing periods as we previously reported (Hao et al., 2015). All animal behaviors were performed in male (4 months old) and female (4 or 6 months old) mice, respectively.

Open field. The open field apparatus consists of a clear, open Plexiglas box (40 × 40 × 30 cm, Stoelting) with overhead camera and photograph beams to record horizontal and vertical movements. Activity was tracked and quantified over a 30-min period by ANY-maze (Stoelting).

Fear conditioning. Fear conditioning was performed to evaluate hippocampus-dependent contextual fear memory and hippocampus-independent cued fear memory (Hao et al., 2015). Briefly, on day 0 animals were trained in a chamber with a grid floor that could deliver an electric shock (Med Associates). This enclosure was put in a sound-attenuating box that contained a digital camera, a loudspeaker, and a house light. Each mouse was placed in the chamber for 2 min during which mice were actively exploring the new environment, after which a tone (30 s, 5 kHz, 80 dB) coincided with a scrambled foot shock (2 s, 0.7 mA). The tone/foot-shock stimuli were repeated once after 1 min. After an additional 1 min, the mouse was removed and returned to its home cage. Fear memory retention was evaluated 24 h after training. The mice were first recorded for 5 min in the same chamber (fresh with 70% ethanol) without tone. Then, they were tested in a novel cage (cleaned with 1% acetic acid) where a 5-min tone was presented after the animals had acclimated to the cage for 5 min. Mouse behavior was recorded and scored automatically by ANY-maze tracking system (Stoelting). Freezing, defined as an absence of all movement except for respiration (Maren et al., 1994), was scored only if the animal was immobile for at least 1 s (Corcoran and Maren, 2001). The percentage of freezing time during the tests serves as an index of fear memory. Cued fear memory was the subtraction of freezing time between the tone phase and the no-tone phase. The preshock immobilization level was normalized from the 2-min baseline before the first foot shock. The postshock freezing level was calculated from the 1 min immediately after the second foot shock (see Fig. 1A). One week after the fear conditioning training, animals were placed back to the fear conditioning chamber for the test of pain threshold of the electric foot shock. Every 30 s, a 2-s scrambled electric foot shock with 0.05 mA increments (starting from 0 mA) was applied. The shock current thresholds of flinch, vocalization, and jumping responses were each recorded (Hao et al., 2015).

Passive avoidance. The passive avoidance assay evaluates associative learning and memory (Samaco et al., 2013). The test apparatus consists of a light and a dark compartment with a guillotine door, across which mice can pass. During the training session, mice were placed into the light compartment and their latency to enter the dark compartment was timed. Immediately after the mice entered the dark compartment with all four paws, the door was shut and an unavoidable foot shock (0.4 mA, 2 s) was delivered. Then the mice were removed to home cage after 10 s. After 24 h, each mouse was placed into the light compartment again and the latency to enter the dark compartment was recorded to measure the retention memory. The maximum cutoff latency was 300 s.

Morris water maze. The Morris water maze was used to assess spatial learning and memory (Moy et al., 2007; Hao et al., 2015). The pool (120 cm in diameter) was filled with water (50 cm deep, 22°C–24°C) made opaque with nontoxic white tempera paint. Visual cues were set on the wall of the testing room, at least 1 m from the pool edge. The ANY-maze tracking system (Stoelting) was used to track and analyze animal swimming. Mice were trained for their ability to find an escape platform (10 cm in diameter) on three different components of the test in turn: hidden platform acquisition, subsequent probe trial in the absence of the platform, and visible platform acquisition. In the hidden platform acquisition training, each animal was given four trials of swimming, a maximum of 60 s for each trial, to find a hidden escape platform cued by visual cues for 9 d. Twenty-four hours after the last training trial of day 9, all the mice were given a probe trial. During the probe trial, the platform was removed, and each animal was allowed 60 s to search in the pool. The amount of time that each animal spent in each quadrant was recorded, as well as the number of times a mouse crossed the imaging location of the platform during training (platform crossings). Another 24 h after the probe test, all the mice received 1-d visible platform training to swim to an escape platform with a visible cue on the platform (above the surface of the water).

Surgery and DBS

Similar to our previous report (Hao et al., 2015), female *Cdkl5*^{+/-} mice and WT littermates (4.5 months old) were secured on a stereotaxic frame (David Kopf) under 1%–2% isoflurane anesthesia. Bipolar DBS electrodes were constructed with Teflon-coated tungsten wire (bare

diameter 50 μm , A-M Systems) and the two tips were horizontally separated by 0.1–0.15 mm. The electrodes were targeted unilaterally to the fimbria-fornix (0.20 mm posterior, 0.24 mm lateral, and 2.3 mm below the bregma) under the guidance of evoked potentials recorded in the ipsilateral DG (1.8–2.0 mm posterior, 1.4–1.6 mm lateral of bregma, 2.2–2.3 mm below the skull) (Paxinos and Franklin, 2001). All the electrodes together with the attached connector sockets were fixed on the skull by dental cement. Animals were given at least 2 weeks to recover.

After recovery, animals were assigned into four groups, respectively: *Cdkl5*^{+/+}-sham, *Cdkl5*^{+/+}-DBS, *Cdkl5*^{+/-}-sham, and *Cdkl5*^{+/-}-DBS. Mice were randomly assigned to DBS or sham groups within the same genotype. Animals in the 2 DBS groups received 1 h DBS daily for 14 consecutive days. The chronic DBS was biphasic rectangular pulses (130 Hz, 60 μs pulse duration), and the stimulus intensities were individually optimized to 80% of the threshold that elicits an after discharge in the hippocampus. Animals in the sham groups experienced the same procedures as those in the DBS groups except for DBS treatment. There was a 3-week interval between the last DBS administration and the beginning of fear conditioning, *in vivo* LTP, or *in vivo* feedforward/feedback inhibition test.

After finishing all experiments, mice were killed with an overdose of isoflurane. An anodal current (30 μA , 10 s) was passed through the electrode wire to verify the electrode placements. Frozen 30 μm coronal sections were cut and stained with cresyl violet for histologic examination.

In vivo electrophysiology

Surgery. Mice were secured on a stereotaxic frame (David Kopf) under 1%–2% isoflurane anesthesia. The stimulating and recording electrodes were surgically implanted as previously described (Tang and Dani, 2009; Hao et al., 2015) with the following modification. Under the guidance of evoked potentials recorded in the DG (1.8–2.0 mm posterior, 1.4–1.6 mm lateral of bregma, 2.2–2.3 mm below the skull), a concentric stimulating electrode was implanted ipsilaterally in the medial PP (0.2 mm posterior and 2.8–3.0 mm lateral of lambda, 1.0–1.3 mm below the dura). The final depth of the electrodes was determined by electrophysiological guidance. A cortical silver ball, placed contralaterally, served as a recording reference as well as ground. Dental cement was used to anchor the electrode assembly that was connected to a 10 \times gain preamplifier and then the connecting device during chronic recordings. Animals were given at least 2 weeks to recover.

Feedforward inhibition. Monophasic square pulses (0.1 ms duration) were delivered to the medial PP. Signals were amplified (100 \times), filtered (bandpass, 0.1–5 kHz), digitized at 10 kHz, and stored on disk for offline analysis (pClamp10 and Digidata 1440A, Molecular Devices). The frequency-dependent inhibition (FDI) was determined as described previously (Sloviter, 1991; Rosenblum et al., 1999; Zhang et al., 2010). Briefly, 10 stimuli at 0.1 Hz followed by 10 stimuli at 1.0 Hz were applied at 40% of the maximal population spike amplitude, and this pattern was repeated once. The population spike amplitude of responses 2–4 at 0.1 Hz stimulation was averaged and compared with the averaged amplitude of last three responses at 1.0 Hz stimulation in each set (see Fig. 3B). Then the results of the two sets were averaged to determine the FDI index.

Feedback inhibition. Following previous studies (Andersen et al., 1966; Sloviter, 1991; Zhang et al., 2010), we delivered paired pulses (conditioning and test) with interstimulus interval of 15, 30, 50, 100, or 150 ms at 0.025 Hz to the medial PP (see Fig. 3D). First, the intensity of the test stimulus was adjusted to evoke a population spike with 70%–80% amplitude of the maximum (see Fig. 3D, Test alone). Then the strength of the conditioning pulse was adjusted to evoke 70%–80% inhibition of the test pop spike when using 15 ms interstimulus interval (i.e., 20%–30% of the test response alone). By delivering pairs of the conditioning pulse and test pulse at various interstimulus intervals (15, 30, 50, 100, or 150 ms), the feedback inhibition index was normalized as the percentage of the test pop spike amplitude in each paired response over the amplitude of the test pop spike alone.

***In vivo* LTP.** After recovery from surgical implantation, mice were habituated to the recording system for 4 d before starting the LTP test. For LTP evaluation, test responses elicited by 0.033 Hz monophasic

pulses (0.1 ms duration) were recorded for 20 min on consecutive days at an intensity that evoked 30%–40% of the maximal population spike. Following 2 d of stable baseline, a tetanus (theta burst stimulation) was delivered to the PP for LTP induction. Pulse duration was doubled during tetani, which consisted of six series of six trains of six stimuli at 400 Hz, 200 ms between trains, 20 s between series. Responses were measured for 60 min right after tetanus and again for 20 min at 24, 48, and 120 h after tetanus. Since the latency of the population spike usually decreases following LTP induction, it is impractical to compare the initial slope of the fEPSP before and after LTP induction in awake animals (M. W. Jones et al., 2001; Malleret et al., 2001). Accordingly, we quantified the amplitude of the population spikes to evaluate LTP (Tang and Dani, 2009; Hao et al., 2015). Data were averaged every 5 min and normalized to the baseline measured over the 10 min before tetanic stimulation.

Ex vivo electrophysiology

Acute brain slice preparation. Acute hippocampal slices were prepared from 4-month-old male *Cdkl5*^{-/-} mice and *Cdkl5*^{+/-} littermates. Animals were deeply anesthetized with isoflurane and decapitated. The brains were quickly removed and transferred to the cold (0°C–4°C) oxygenated cutting solution containing the following (in mM): 93 NMDG, 93 HCl, 2.5 KCl, 1.2 NaH₂PO₄, 30 NaHCO₃, 20 HEPES, 25 glucose, 5 sodium ascorbate, 2 thiourea, 3 sodium pyruvate, 10 MgSO₄, and 0.5 CaCl₂, pH 7.4. Each brain was separated into halves by a sagittal cut at the midline. Then, coronal slices (300 μm thickness) containing the dorsal hippocampus were cut with a vibratome (Leica Microsystems) at a speed of 0.18 mm/s. Slices were then transferred to ACSF containing the following (in mM): 125 NaCl, 2.5 KCl, 1.5 MgCl₂, 2 CaCl₂, 25 D-glucose, 25 NaHCO₃, and 1.25 NaH₂PO₄, pH 7.4, incubated at 37.0 \pm 0.5°C for 15–30 min and then at room temperature (20°C–22°C) for 0.5–1 h before recordings.

Whole-cell recordings. Individual slices were transferred to a submerged chamber that was perfused with oxygenated ACSF at a rate of 2 ml/min. The whole-cell patch-clamp recordings were performed under room temperature from the soma of DG granule cells (DGCs) and MOPP cells in the molecular layer of the DG. Signals were acquired with a Multiclamp 700B amplifier (Molecular Device), filtered between 1 Hz and 5 kHz, and digitized at 20 kHz with a Digidata-1550 system (Molecular Devices). Data acquisition and offline analysis were performed with Clampfit 10.6 software (Molecular Devices). Recording pipettes (6–9 M Ω , filled with intracellular solution) were pulled from borosilicate glass capillaries (B200-116-10, Sutter Instrument) using a horizontal glass electrode puller (P-1000, Sutter Instrument). Cell capacitance and membrane input resistance were determined in whole-cell voltage-clamp mode with a depolarizing step voltage command (10 mV) by using the membrane test function integrated in the Clampex software after the whole-cell patch-clamp configuration was achieved. The access resistance ranged from 10 to 30 M Ω and was periodically monitored and only neurons within a change of access resistance <15% during the experiments were used for further analysis.

Intrinsic membrane/firing properties were acquired in current-clamp mode with an intracellular recording pipette solution containing the following (in mM): 120 potassium gluconate, 10 HEPES, 4 KCl, 4 MgATP, 0.4 Na₃GTP, and 10 sodium phosphocreatine, pH 7.25 (adjusted with KOH). A series of current steps (1000 ms) were presented in ascending order (50 pA step) from –200 pA to 500 pA every 10 s to analyze the membrane and firing properties of neurons.

sEPSCs and sIPSCs were recorded in voltage-clamp with intracellular solution containing the following (in mM): 125 Cs-methanesulfonate, 1 EGTA, 2.5 MgCl₂, 4 MgATP, 0.4 Na₃GTP, 10 sodium phosphocreatine, 10 HEPES, and 2 QX-314, pH 7.25 (adjust with CsOH). To assess sEPSCs, cells were recorded in the presence of 25 μM bicuculline. sIPSCs were collected in the presence of CNQX (20 μM) and D-AP5 (25 μM). sEPSCs and sIPSCs were isolated by clamping neurons at –60 mV and 10 mV, which are in very close proximity to the reversal potential for GABA_ARs and AMPARs, respectively (Allene et al., 2012). In some experiments, biocytin (0.5%, Sigma) was added to the intracellular solution to identify the location of recorded cells.

We measured evoked EPSCs (eEPSCs) in the DGCs and MOPP cells received from the PP by dual voltage-clamp. A concentric bipolar stimulating microelectrode with a cone tip 25 μm in diameter (30202, FHC) was placed within the middle one-third of the DG molecular layer, \sim 50–100 μm to the target neurons. The position of the stimulating microelectrode was carefully adjusted to evoke responses simultaneously in DGCs and MOPP cells. This setting avoided the direct activation of the hilar commissural pathway from the contralateral mossy cells that innervate the inner one-third of the DG molecular layer. A dual voltage-clamp technique allowed us to directly compare the synaptic input on the DGCs and MOPP cells induced by the same group of PP fibers from the entorhinal cortex. Stimuli were delivered every 15 s, with intensity ranging from 10 to 110 μA (increasing in increments of 5 μA), and two trials for each intensity. To estimate presynaptic neurotransmitter release, paired-pulse stimuli with 50 ms interstimulus interval were delivered to the medial PP every 15 s for 5 trials. The amplitude of the second response was divided by the amplitude of the first response within a pair to get the paired-pulse ratio (PPR). PPRs in MOPP cells and DGCs were calculated as the mean ratio of the 5 paired stimulus trials, respectively. To measure the size of readily releasable pool (RRP) and the vesicle release probability (P_{ves}), cells were held at -60 mV and 60 stimuli were delivered at 20 Hz for 3 s with an intensity adjusted to evoke 70% of the maximal eEPSC amplitude. Peak amplitudes of eEPSCs are measured and cumulated. A straight line was fitted to the final 15 points of the cumulative eEPSCs and back-extrapolated to the y axis. The Y intercept corresponds to RRP size, and P_{ves} equals the amplitude of the first eEPSC divided by RRP size, as previously described (Schneppenburger et al., 1999).

To measure AMPAR and NMDAR-mediated current ratio, stimulus intensity was set to result in 90% of maximal eEPSC. Both DGCs and MOPP cells were first held at a holding potential of -60 mV to record evoked AMPAR-mediated EPSCs (AMPA-EPSCs). The holding potential was then changed to 40 mV for granule cells and 60 mV for MOPP cells to record eEPSCs mediated by AMPAR and NMDAR. The amplitude of eEPSC 50 ms after the stimulus was considered to be the NMDAR-mediated component of EPSC (NMDA-EPSCs), since the AMPA EPSCs fade because of their unique channel property (Umehiya et al., 1999; Etherton et al., 2011). For each cell, at least 10 trials were averaged to obtain a representative response at each holding potential. To calculate the AMPA/NMDA ratio in DGCs and MOPP cells, the peak amplitude of the AMPA-EPSC at -60 mV was divided by the NMDA-EPSC amplitude at 40 or 60 mV, respectively.

Immunohistochemistry

The whole-cell patch recorded slices were fixed in 4% PFA for 3–5 h and transferred into 30% sucrose overnight. These slices were washed 3 times in PBS (10 min each) before being treated with Cy5 conjugate of streptavidin (1:1000, Thermo Fisher Scientific) diluted in PBS containing 5% serum and 1% Triton X-100 for 3 h. Slices were then counterstained with DAPI (900 nM, D1036, Invitrogen) for 15 min at room temperature in darkness. After washing the slices with 0.1 M PBS 3 times, we mounted them on glass slides with Fluoromount-G (Southern Biotechnology). Images were obtained with Carl Zeiss 880 confocal microscope using a 20 \times dry objective to identify the recorded cells.

Intracranial drug infusion

Under aseptic conditions, custom-made 26G guide cannulas were implanted bilaterally (2.0 mm posterior, 1.0 mm lateral, and 0.9 mm below the bregma) in *Cdkl5*^{-/-} mice and littermate *Cdkl5*^{+/-} controls anesthetized with isoflurane. After 2 weeks of recovery, mice of each genotype were randomly assigned into drug- or vehicle-treated groups. Gabazine hydrobromide (Sigma, SR-95531) was dissolved in PBS, pH 7.4, and the solution was back-filled into a 33G injector that was lowered 1.0 mm below the guide cannula tip while in place. The solution of 0.5 μl drug (1.0 ng gabazine, based on literature [Lu et al., 2016] and our pilot tests) or PBS vehicle per side was microinfused over 1 min into the dorsal hippocampus through a pump (Harvard Apparatus) (Tang and Dani, 2009; Hao et al., 2015). The injection sites in the hippocampi were aimed to the molecular layer of the DG where the MOPP cells locate. Following

each injection, the injector was left in place for an additional minute to allow drug diffusion. To determine the effect of gabazine on hippocampus-dependent memory, animals that received gabazine or vehicle were transferred into a fear conditioning chamber \sim 15 min after the injection. The fear conditioning training and 24 h retention tests of contextual and cued fear memory were conducted as described under Behavioral assays. For histologic verification of the injection sites, 4% methylene blue in PBS (\sim 0.2 μl) was injected into each injection site at the end of the experiment. The mice were killed with an overdose of isoflurane and their brains dissected. Frozen 30 μm coronal sections were cut and costained with cresyl violet and eosin. One mouse with injection sites outside of the targeted brain regions was excluded from data analysis.

Experimental design and statistical analysis

For behavioral assays, we determined sample sizes based on previously published results in this CDD model (Wang et al., 2012). For *in vivo* electrophysiology, we chose sample sizes and power based on our previous publications (Zhang et al., 2010; Hao et al., 2015). Mice within the same genotype were randomly assigned to receive DBS or drug treatment. For *ex vivo* electrophysiological experiments, sample sizes were determined based on previous publications (Wang et al., 2017a,b) and reported as the numbers of cells/mouse.

All data were analyzed using the Shapiro–Wilk test for normality. For two-sample comparisons, datasets with normal distributions were analyzed for significance using two-tailed unpaired or paired t test, whereas datasets with non-normal distributions were analyzed using the Mann–Whitney test. One-way or two-way repeated-measures ANOVA and two-way ANOVA were conducted as appropriate. If any of the main effects were significant, the Tukey *post hoc* test was used for all pairwise multiple comparisons. Significance was defined as $p < 0.05$. Data in line plots and in the text are presented as mean \pm SEM. In box plots, horizontal lines are the median and the 25% and 75% range values; whiskers present the extreme data points from the box edges. Sample sizes and statistical details of each experiment can be found in Results. GraphPad Prism 8 was used to create all the plots and the statistical tests in this study.

Results

Loss of CDKL5 impairs hippocampus-dependent learning and memory

To explore the effects of CDKL5 deficiency on hippocampal memory in the mouse model used in this study (B6.129(FVB)-*Cdkl5*^{tm1.1Joeez/J}), we performed multiple behavioral assays in both male (*Cdkl5*^{-/-}) and female (*Cdkl5*^{+/-}) mutant mice and their sex- and age-matched WT littermate controls (WT, *Cdkl5*^{+/-} or *Cdkl5*^{+/+}). We first conducted the classic fear conditioning task (Fig. 1A). Because CDKL5-deficient mice tend to show more motor activity (Extended Data Fig. 1–1), we first established that, during fear conditioning training, 4-month-old *Cdkl5*^{-/-} mice showed similar levels of exploration before the foot shock as their WT littermates (*Cdkl5*^{-/-} 0.38 \pm 0.21% vs *Cdkl5*^{+/-} 0.34 \pm 0.21%, Mann–Whitney test, $U = 67.5$, $p = 0.745$, preshock data in Fig. 1B). The mutant animals froze less, however, immediately after the foot shock (*Cdkl5*^{-/-} 22.40 \pm 3.64% vs *Cdkl5*^{+/-} 37.54 \pm 3.80%, two-tailed unpaired t test, $t_{(22)} = 3.800$, $p = 0.0088$) compared with WT littermates (postshock data in Fig. 1B). Consistent with previous fear conditioning study results (Wang et al., 2012), *Cdkl5*^{-/-} mice froze less in both the conditioning context and the cued novel environment than did controls when tested 24 h after fear conditioning training (contextual: *Cdkl5*^{-/-} 17.50 \pm 2.70% vs *Cdkl5*^{+/-} 29.37 \pm 4.44%, two-tailed unpaired t test, $t_{(22)} = 2.284$, $p = 0.0324$; cued: *Cdkl5*^{-/-} 32.89 \pm 3.86% vs *Cdkl5*^{+/-} 57.25 \pm 5.93%, Mann–Whitney test, $U = 29.0$, $p = 0.0140$; Fig. 1C,D). During a passive avoidance task, in which we trained the mice to avoid a dark compartment by giving a foot shock (Samaco et al., 2013), the male mutant mice entered the shock compartment more quickly than

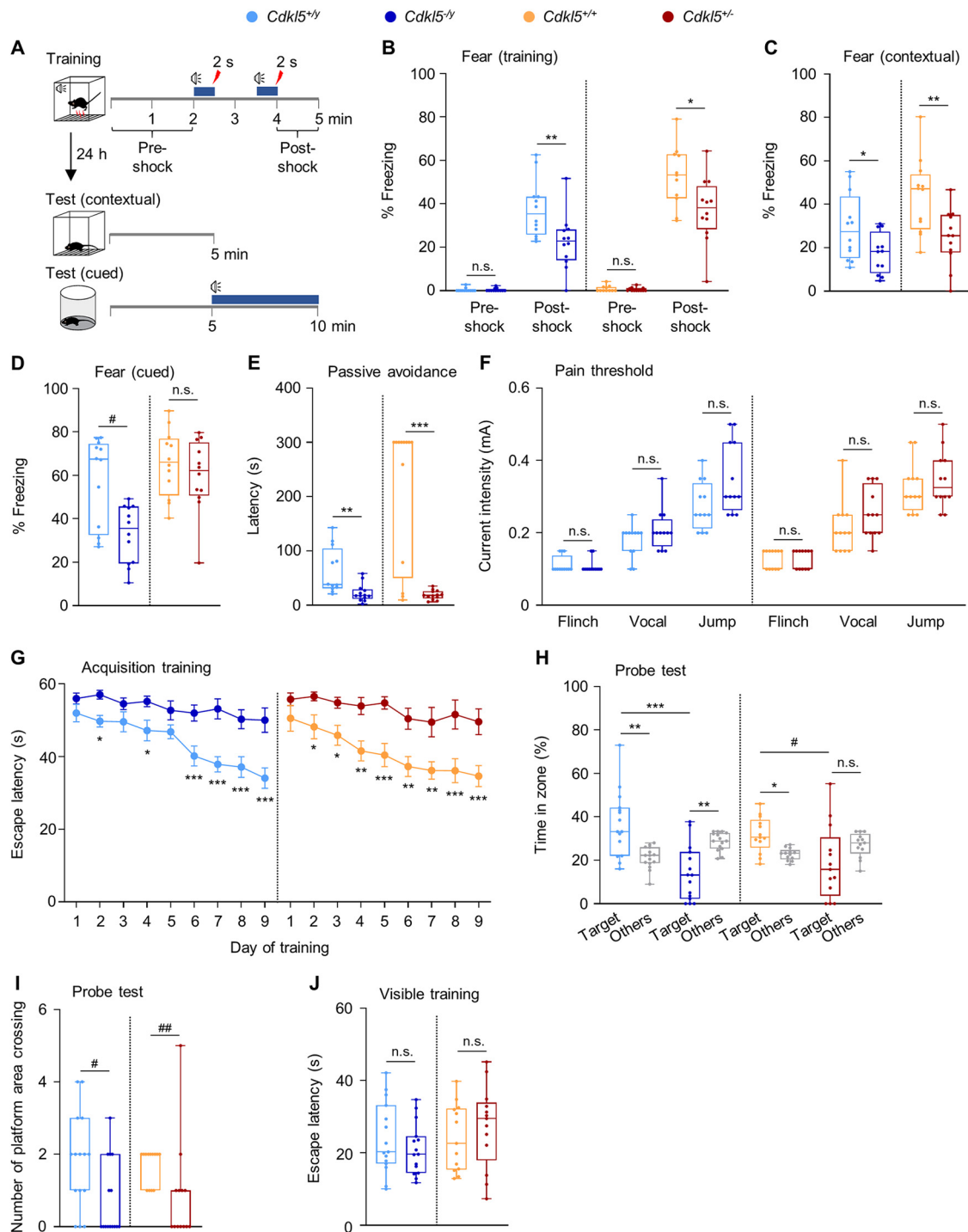


Figure 1. Loss of CDKL5 impairs hippocampus-dependent learning and memory in male *Cdkl5*^{-/-} and female *Cdkl5*^{+/-} mice. **A–D**, Learning and memory in the fear conditioning task in 4-month-old male *Cdkl5*^{-/-} mice and 6-month-old female *Cdkl5*^{+/-} mice (dark blue and red, respectively), together with their age- and sex-matched WT littermates (*Cdkl5*^{+/+}, *Cdkl5*^{+/-}; light blue and orange, respectively) ($n = 12$ mice per group). **A**, Schematic representation of fear conditioning paradigm. **B**, During fear conditioning training, both male and female mutant mice showed comparable exploration levels before the first foot shock compared with their WT littermates, respectively. However, both male and female mutant mice froze less than their WT littermates immediately after the second foot shock. **C**, Both male and female mutant mice showed less freezing in response to the contextual fear conditioning than their WT littermates. **D**, *Cdkl5*^{-/-} mice showed less freezing in response to the cued fear conditioning than their WT littermates, whereas *Cdkl5*^{+/-} mice showed comparable cued freezing level as their WT littermates. **E**, Both male *Cdkl5*^{-/-} mice ($n = 12$) at 4 months of age and female *Cdkl5*^{+/-} mice ($n = 13$) at 6 months of age showed less hesitation to enter the dark compartment in the passive avoidance task than their age- and sex-matched WT littermates (*Cdkl5*^{+/+}, $n = 13$; *Cdkl5*^{+/-}, $n = 13$). **F**, There was no difference in pain threshold intensities to evoke flinch, vocalization, or jumping between male *Cdkl5*^{-/-} mice and *Cdkl5*^{+/+} littermates or between female *Cdkl5*^{+/-} mice and *Cdkl5*^{+/+} controls ($n = 12$ per group). **G–J**, Learning and memory in the water maze task in male *Cdkl5*^{-/-} mice ($n = 15$) at 4 months of age and female *Cdkl5*^{+/-} mice ($n = 13$) at 6 months of age, together with their age- and sex-matched WT littermates (*Cdkl5*^{+/-}, $n = 13$; *Cdkl5*^{+/+}, $n = 13$). **G**, Escape latency during acquisition training. The mutant mice did not show much improvement during the training. **H**, Percentage of time in the target zone and averaged time in other zones during probe test. **I**, Number of platform area crossings in the probe test. **J**, Escape latency in the water maze task with a flagged platform. * $p < 0.05$, ** $p < 0.01$, *** $p < 0.001$; # $p < 0.05$, ## $p < 0.01$, Mann–Whitney test. For details on locomotor activity in both male and female *Cdkl5* mutant mice as well as memory performances in 4-month-old female *Cdkl5*^{+/-} mice and *Cdkl5*^{+/+} controls, see Extended Data Figures 1-1 and 1-2.

controls ($Cdkl5^{-/-}$ 22.48 ± 4.46 vs $Cdkl5^{+/y}$ 62.87 ± 12.16 , two-tailed unpaired t test, $t_{(23)} = 3.218$, $p = 0.0038$; Fig. 1E), indicating impaired hippocampal memory. There was no difference in pain threshold between genotypes (current intensity for flinch: $Cdkl5^{-/-}$ 0.11 ± 0.006 vs $Cdkl5^{+/y}$ 0.11 ± 0.007 , Mann–Whitney test, $U = 66.0$, $p = 0.6520$; vocalization: $Cdkl5^{-/-}$ 0.21 ± 0.02 vs $Cdkl5^{+/y}$ 0.18 ± 0.01 , two-tailed unpaired t test, $t_{(22)} = 1.410$, $p = 0.1720$; jump: $Cdkl5^{-/-}$ 0.35 ± 0.03 vs $Cdkl5^{+/y}$ 0.28 ± 0.02 , Mann–Whitney test, $U = 39.0$, $p = 0.0550$; Fig. 1F).

We next used a water maze task to test spatial learning and memory (Morris et al., 1982; Hao et al., 2015). The $Cdkl5^{-/-}$ mice took longer to locate the platform during training than their WT littermates (two-way repeated-measures ANOVA followed by Tukey's *post hoc* analysis: genotype, $F_{(1,28)} = 29.66$, $p < 0.001$; day, $F_{(8,224)} = 8.35$, $p < 0.001$; genotype \times day interaction, $F_{(8,224)} = 2.23$, $p = 0.0260$; Fig. 1G). When we removed the platform during the probe trial, the mutant mice could not remember the platform location and spent less time in the target quadrant ($Cdkl5^{-/-}$ target 36.63 ± 3.90 vs $Cdkl5^{+/y}$ others 21.12 ± 1.30 , two-tailed paired t test, $t_{(14)} = 2.981$, $p = 0.0099$; $Cdkl5^{-/-}$ target 13.86 ± 3.29 vs $Cdkl5^{-/-}$ others 28.73 ± 1.10 , two-tailed paired t test, $t_{(14)} = 3.386$, $p = 0.0044$; $Cdkl5^{-/-}$ target 13.86 ± 3.29 vs $Cdkl5^{+/y}$ target 36.63 ± 3.90 , two-tailed unpaired t test, $t_{(28)} = 4.460$, $p = 0.0001$; Fig. 1H). As a result, $Cdkl5^{-/-}$ mice swam through the area where the platform had been less frequently ($Cdkl5^{-/-}$ 0.73 ± 0.27 vs $Cdkl5^{+/y}$ 1.80 ± 0.34 , Mann–Whitney test, $U = 60.0$, $p = 0.0240$; Fig. 1I). This poor performance was not because of differences in visual or sensorimotor skills (escape latency during visible training: $Cdkl5^{-/-}$ 20.99 ± 1.83 vs $Cdkl5^{+/y}$ 23.93 ± 2.54 , two-tailed unpaired t test, $t_{(28)} = 0.939$, $p = 0.3560$; Fig. 1J).

Although CDD primarily affects human females, there have been fewer studies done with female $Cdkl5^{+/y}$ mice because CDKL5 is on the X chromosome and thus is expressed mosaically (so the phenotype would be milder and later-onset than in males); skewed X-chromosome inactivation could also make the results less predictable. Nevertheless, because female $Cdkl5^{+/y}$ mice are more clinically relevant, we subjected them to the same behavioral tests to evaluate learning and memory. During fear conditioning training, 4-month-old female mice showed similar levels of exploratory behavior before the foot shock but froze less immediately after the foot shock compared with WT littermates (Extended Data Fig. 1-2A). These female mutant mice did not show memory deficits in either contextual or cued fear conditioning (Extended Data Fig. 1-2B,C) or the passive avoidance task (Extended Data Fig. 1-2D) when tested 24 h later.

To determine whether the fear-conditioned memory impairment in female $Cdkl5$ heterozygous mice is affected by aging, we tested hippocampal memory in an older cohort of mice. Similar to the younger mice, 6-month-old female mutant mice showed comparable exploratory behavior before the foot shock ($Cdkl5^{+/y}$ $0.51 \pm 0.25\%$ vs $Cdkl5^{+/+}$ $0.84 \pm 0.41\%$, Mann–Whitney test, $U = 59.5$, $p = 0.664$) and froze less immediately following the foot shock ($Cdkl5^{+/y}$ $37.17 \pm 4.38\%$ vs $Cdkl5^{+/+}$ $52.64 \pm 4.25\%$, two-tailed unpaired t test, $t_{(21)} = 2.536$, $p = 0.0196$) compared with WT littermates (Fig. 1B). In contrast to the younger female mutant mice, 6-month-old female heterozygous mice did display contextual memory deficits (contextual: $Cdkl5^{+/y}$ $24.81 \pm 3.73\%$ vs $Cdkl5^{+/+}$ $43.68 \pm 5.00\%$, two-tailed unpaired t test, $t_{(22)} = 3.024$, $p = 0.0062$; cued: $Cdkl5^{+/y}$ $59.86 \pm 4.84\%$ vs $Cdkl5^{+/+}$ $65.68 \pm 4.42\%$, two-tailed unpaired t test, $t_{(22)} = 0.887$, $p = 0.3840$; Fig. 1C,D). In the passive avoidance task, the 6-month-old female mutant mice entered the shock compartment much earlier than did the WT controls ($Cdkl5^{+/y}$ 18.87 ± 2.33 vs $Cdkl5^{+/+}$ 214.23 ± 35.59 , two-

tailed unpaired t test, $t_{(24)} = 5.478$, $p = 0.00001$; Fig. 1E). Again, there was no difference of pain threshold between genotypes (current intensity for flinch: $Cdkl5^{+/y}$ 0.13 ± 0.007 vs $Cdkl5^{+/+}$ 0.13 ± 0.007 , Mann–Whitney test, $U = 72.0$, $p = 1.0000$; vocalization: $Cdkl5^{+/y}$ 0.25 ± 0.02 vs $Cdkl5^{+/+}$ 0.21 ± 0.02 , Mann–Whitney test, $U = 45.5$, $p = 0.1210$; jump: $Cdkl5^{+/y}$ 0.35 ± 0.02 vs $Cdkl5^{+/+}$ 0.33 ± 0.02 , two-tailed unpaired t test, $t_{(22)} = 0.692$, $p = 0.4960$; Fig. 1F).

Like the male $Cdkl5$ null mice in the water maze task, female $Cdkl5^{+/y}$ mice took longer to find the platform over the acquisition sessions than did their WT littermates (two-way repeated-measures ANOVA followed by Tukey's *post hoc* analysis: genotype, $F_{(1,24)} = 27.32$, $p < 0.001$; day, $F_{(8,192)} = 5.38$, $p < 0.001$) and did not show a preference for the target quadrant (Fig. 1G). As a result, $Cdkl5^{+/y}$ mice spent less time in the target quadrant ($Cdkl5^{+/y}$ target 31.76 ± 2.28 vs $Cdkl5^{+/+}$ others 22.74 ± 0.76 , two-tailed paired t test, $t_{(12)} = 2.973$, $p = 0.0116$; $Cdkl5^{+/y}$ target 18.78 ± 4.70 vs $Cdkl5^{+/+}$ others 27.08 ± 1.57 , two-tailed paired t test, $t_{(12)} = 1.323$, $p = 0.2100$; $Cdkl5^{+/y}$ target 18.78 ± 4.70 vs $Cdkl5^{+/+}$ target 31.76 ± 2.28 , Mann–Whitney test, $U = 38.0$, $p = 0.0180$; Fig. 1H) and swam over the platform area fewer times than did their WT counterparts ($Cdkl5^{+/y}$ 0.85 ± 0.39 vs $Cdkl5^{+/+}$ 1.69 ± 0.13 , Mann–Whitney test, $U = 29.5$, $p = 0.0030$; Fig. 1I) during the probe trial. Their visual and sensorimotor skills were normal (escape latency during visible training: $Cdkl5^{+/y}$ 27.20 ± 3.14 vs $Cdkl5^{+/+}$ 24.22 ± 2.56 , two-tailed unpaired t test, $t_{(24)} = 0.735$, $p = 0.4690$; Fig. 1J).

CDKL5 loss impairs hippocampal synaptic plasticity and inhibitory activity in freely moving mice

The clear hippocampus-dependent memory impairment in $Cdkl5$ mutant mice led us to examine synaptic plasticity of the PP to the DG. Given that LTP of synaptic transmission serves as a neural substrate for learning and memory (Malenka and Bear, 2004; Whitlock et al., 2006), we expected that LTP would be impaired. We therefore implanted stimulation electrodes in the medial PP and recording electrodes in the ipsilateral DG in both male $Cdkl5^{-/-}$ and female $Cdkl5^{+/y}$ mice and their WT littermates at the ages they displayed impaired memory. After 2 d of baseline recordings, we used theta burst stimulation to induce LTP and monitored the responses for 5 d while they moved freely, as previously described (Hao et al., 2015). Both $Cdkl5^{-/-}$ mice and their $Cdkl5^{+/y}$ littermates showed LTP (one-way repeated-measures ANOVA on day 0: $Cdkl5^{+/y}$, $F_{(15,135)} = 29.74$, $p < 0.001$; $Cdkl5^{-/-}$, $F_{(15,90)} = 26.32$, $p < 0.001$; Fig. 2A,B). LTP in $Cdkl5^{-/-}$ mice, however, had lower magnitude than in controls. Two-way repeated-measures ANOVA revealed a significant genotype effect last for 3 d after induction (day 0, $F_{(1,14)} = 13.41$, $p = 0.0030$; day 1, $F_{(1,13)} = 7.63$, $p = 0.0160$; day 2, $F_{(1,13)} = 5.94$, $p = 0.0300$; Fig. 2B).

Similarly, theta burst stimulation induced LTP in both $Cdkl5^{+/y}$ mice (one-way ANOVA on day 0, $F_{(15,90)} = 13.24$, $p < 0.001$) and WT controls ($F_{(15,90)} = 26.50$, $p < 0.001$; Fig. 2A, C). The heterozygous female mice had impaired LTP for at least 2 d after induction (two-way repeated-measures ANOVA, genotype effect: day 0, $F_{(1,12)} = 5.42$, $p = 0.0380$; day 1, $F_{(1,12)} = 8.37$, $p = 0.014$; day 2, $F_{(1,12)} = 3.95$, $p = 0.070$; Fig. 2C). Therefore, complete loss of CDKL5 in the male nulls or partial loss of CDKL5 in the female heterozygous mice severely impairs synaptic plasticity in the PP-DG pathway. *In vivo* synaptic plasticity in the neural pathway gating cortical information to the hippocampus thus requires CDKL5 protein.

Altered local circuit activity may impair hippocampal memory and synaptic plasticity. Inhibitory interneurons exert powerful

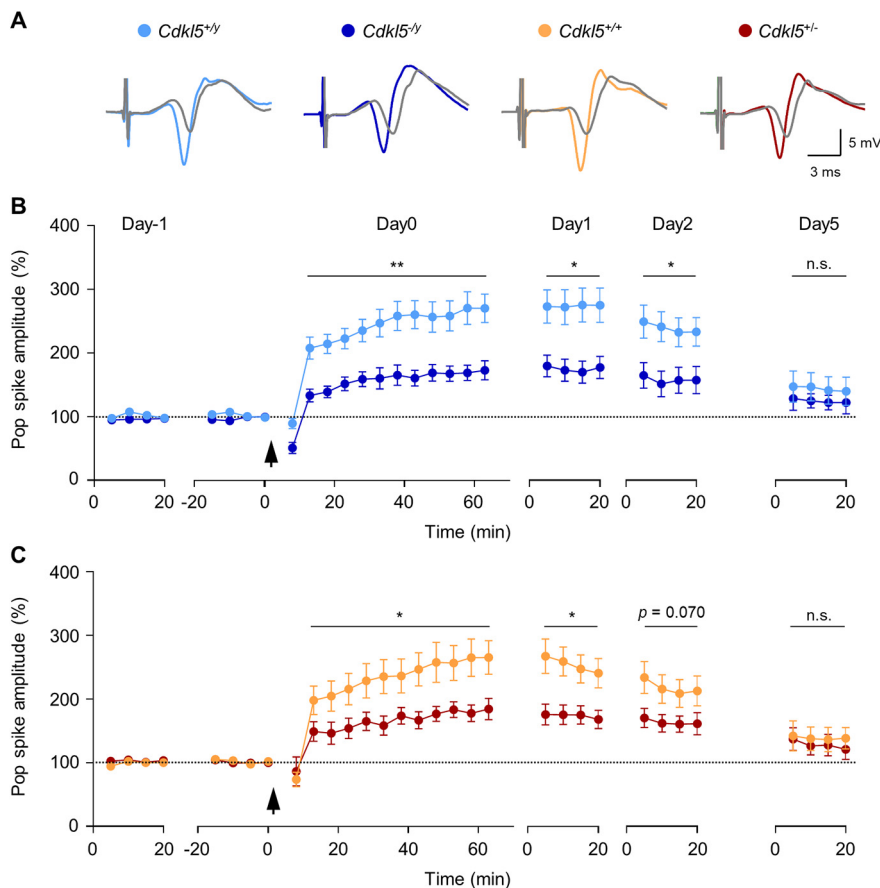


Figure 2. Freely moving *Cdkl5*^{-/-} and *Cdkl5*^{+/-} mice show impaired hippocampal synaptic plasticity in the DG. **A**, Superimposed representative traces of evoked response of the PP recorded in the DG 5 min before (gray) and 55 min after tetani. **B**, Summary of *in vivo* LTP in 4-month-old male *Cdkl5*^{-/-} mice ($n = 6-7$) and *Cdkl5*^{+/-} littermates ($n = 9$). LTP was induced by theta burst stimulation (arrow) on day 0 and followed up for 5 more days. **C**, Summary of *in vivo* LTP in 6-month-old female *Cdkl5*^{+/-} mice ($n = 7$) and *Cdkl5*^{+/+} controls ($n = 7$). LTP was induced by theta burst stimulation (arrow) on day 0 and followed up for 5 more days. * $p < 0.05$, ** $p < 0.01$.

control over local circuit activity (Freund and Buzsáki, 1996). GABAergic interneurons in the DG integrate into the PP-initiated local feedforward and feedback inhibition circuits (Fig. 3A) and play major roles not only in regulating single-cell excitability but in gating, filtering, and processing cortical inputs to the hippocampus (Hsu et al., 2016; Hainmueller and Bartos, 2020). Therefore, we hypothesized that CDKL5 might be critical specifically to the inhibitory circuits that mediate synaptic plasticity and memory function.

To test feedforward inhibition, we applied 10 stimuli at 0.1 Hz followed by 10 stimuli at 1.0 Hz to the medial PP and repeated this pattern once. We normalized the pop spike amplitudes of the resulted responses in the DG to get the FDI index (Rosenblum et al., 1999; Zhang et al., 2010) (Fig. 3B). Compared with their WT littermates, both *Cdkl5*^{-/-} and *Cdkl5*^{+/-} mice had a lower FDI index, indicating increased feedforward inhibition after CDKL5 loss (*Cdkl5*^{-/-} 0.69 ± 0.03 vs *Cdkl5*^{+/-} 0.80 ± 0.03 , two-tailed unpaired *t* test, $t_{(15)} = 2.636$, $p = 0.0187$; *Cdkl5*^{+/-} 0.58 ± 0.05 vs *Cdkl5*^{+/+} 0.74 ± 0.04 , two-tailed unpaired *t* test, $t_{(12)} = 2.700$, $p = 0.0193$; Fig. 3C). To evaluate feedback inhibition, we delivered paired-pulse stimuli (conditioning and test) at varied interstimulus intervals to the medial PP, and then compared the pop spike amplitude of the test responses to the amplitude of the response evoked by single test pulse stimulation (Andersen et al., 1966; Sloviter, 1991; Zhang et al., 2010) (Fig. 3D). As shown

in Figure 3E, there was no difference in feedback inhibition index between mutants and their WT littermates across the interstimulus intervals in both *Cdkl5*^{-/-} mice (two-way repeated-measures ANOVA, genotype effect, $F_{(1,15)} = 0.87$, $p = 0.3660$) and *Cdkl5*^{+/-} animals ($F_{(1,9)} = 0.68$, $p = 0.4320$). These results indicate that CDKL5 loss specifically increases feedforward inhibition in the PP to the DG.

CDKL5 loss alters excitatory and inhibitory synaptic transmission in the *Cdkl5*^{-/-} DG

Several studies have shown altered E/I balance at play in multiple psychiatric and neurodevelopmental disorders (Nelson and Valakh, 2015; Foss-Feig et al., 2017). The DGCs receive both excitatory glutamatergic input from the PP and inhibitory input from local inhibitory GABAergic interneurons. We therefore tested the effect of CDKL5 loss on synaptic transmission of DGCs by recording sEPSCs and sIPSCs in hippocampal slices. Given the confounding effects of mosaic CDKL5 expression in female heterozygous mice from random X-chromosome inactivation, we compared male *Cdkl5* null (*Cdkl5*^{-/-}) mice with their male WT littermates (*Cdkl5*^{+/-}). Both the frequency and amplitude of sEPSCs were lower in *Cdkl5*^{-/-} mice than in WT controls (frequency: *Cdkl5*^{-/-} 0.65 ± 0.05 vs *Cdkl5*^{+/-} 0.98 ± 0.08 , Mann-Whitney test, $U = 252.0$, $p = 0.0020$; amplitude: *Cdkl5*^{-/-} 7.32 ± 0.20 vs *Cdkl5*^{+/-} 8.13 ± 0.24 , two-tailed unpaired *t* test, $t_{(59)} = 2.564$, $p = 0.0129$; Fig. 4A). In contrast, the sIPSC frequency was higher (*Cdkl5*^{-/-} 1.56 ± 0.13 vs *Cdkl5*^{+/-} 0.79 ± 0.0730 , Mann-Whitney test, $U = 89.0$, $p \leq 0.001$), whereas sIPSC amplitude remained the same (*Cdkl5*^{-/-} 13.98 ± 0.92 vs *Cdkl5*^{+/-} 15.10 ± 0.79 , two-tailed unpaired *t* test, $t_{(47)} = 0.925$, $p = 0.3600$; Fig. 4B). These data suggest that DGCs in *Cdkl5*^{-/-} mice receive less excitatory and more inhibitory input, skewing the E/I balance toward inhibition.

We reasoned that this imbalance might originate from interneurons. We were particularly interested in MOPP cells, which contribute the most to feedforward inhibition of DGCs (Li et al., 2013). To determine whether CDKL5 loss enhances the excitatory synaptic transmission from the PP to MOPP cells, which would then increase inhibitory input to the DGCs, we recorded their sEPSCs. As expected, MOPP cells in *Cdkl5*^{-/-} mice displayed higher sEPSC frequency than in *Cdkl5*^{+/-} controls (*Cdkl5*^{-/-} 3.96 ± 0.26 vs *Cdkl5*^{+/-} 2.68 ± 0.19 , Mann-Whitney test, $U = 206.0$, $p \leq 0.001$), but similar amplitude (*Cdkl5*^{-/-} 7.75 ± 0.25 vs *Cdkl5*^{+/-} 7.39 ± 0.24 , two-tailed unpaired *t* test, $t_{(59)} = 1.064$, $p = 0.2920$; Fig. 4C). This supports the notion that increased excitatory input onto MOPP cells led to the increased DGC inhibition we observed in *Cdkl5*^{-/-} mice.

To further probe this model, we performed simultaneous dual patch recordings in MOPP cells and DGCs to get PP-

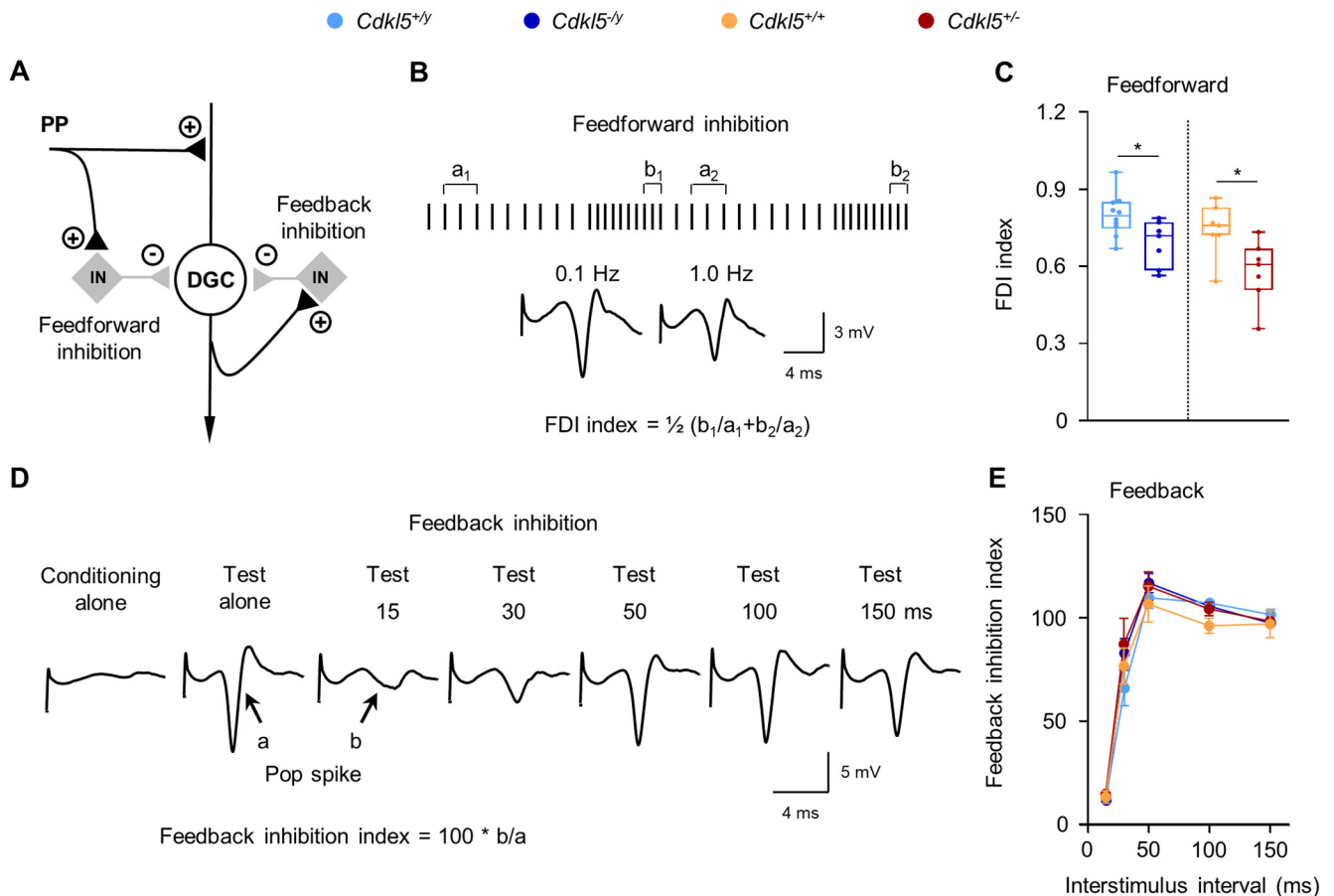


Figure 3. Freely moving *Cdkl5*^{-/-} and *Cdkl5*^{+/-} mice show altered inhibitory circuit activity in the DG. **A**, Diagram of the feedforward and feedback inhibition circuitry in the DG. IN, Interneuron; +, excitatory; -, inhibitory. **B**, The stimulus protocol of FDI was used to determine the feedforward inhibition in the PP to DG pathway. Ten pulses were delivered to the medial PP at 0.1 Hz followed by 10 pulses at 1.0 Hz. This pattern was repeated once. The evoked responses in the ipsilateral dentate were recorded. The population spike amplitudes from the responses 2–4 at 0.1 Hz (*a*₁, *a*₂) were averaged, respectively, and divided the averaged amplitude of the last three responses at 1.0 Hz (*b*₁, *b*₂) in each set. The results of the two sets were averaged to give the FDI index. Representative traces were evoked by 0.1 and 1.0 Hz pulses, respectively. **C**, Summary of the FDI index in male *Cdkl5*^{-/-} mice (*n* = 7) and *Cdkl5*^{+/-} littermates (*n* = 10) as well as female *Cdkl5*^{+/-} mice (*n* = 7) and *Cdkl5*^{+/-} littermates (*n* = 7). Loss of CDKL5 decreased FDI index (for increased feedforward inhibition). **D**, Determination of feedback inhibition. Field potential recordings (average of 10 traces collected at 0.025 Hz) were recorded from the dentate in response to the ipsilateral paired stimuli of the medial PP. The examples showed the responses evoked by conditioning stimulus alone, test stimulus alone, and the test responses evoked by paired stimuli (conditioning + test) at different interstimulus intervals (15, 30, 50, 100, and 150 ms). **E**, Normalized feedback inhibition index versus interstimulus interval plot in male *Cdkl5*^{-/-} mice (*n* = 7) and *Cdkl5*^{+/-} littermates (*n* = 10) as well as female *Cdkl5*^{+/-} mice (*n* = 5) and *Cdkl5*^{+/-} littermates (*n* = 6). **p* < 0.05.

induced evoked responses. Placing a fine-tipped (25 μ m in diameter) concentric bipolar stimulating electrode in the middle one-third of the DG molecular layer (Fig. 4D) allowed us to stimulate only the medial PP and avoid activating other synaptic input to the MOPP cells and DGCs (Hsu et al., 2016). In a few cases, the dual patch proved a direct connection between MOPP cells and DGCs. Activation of the MOPP cell evoked an inhibitory postsynaptic potential in the paired DGC with a \sim 10 ms latency (Fig. 4E,F), confirming that the recorded MOPP cell mediated feedforward inhibition from the PP to the DGC. We conducted pairwise analysis on evoked responses over incremental stimulus intensities (input-output curve). The eEPSC amplitude in MOPP cells was significantly larger than that of DGCs in *Cdkl5*^{+/-} mice, indicating that the MOPP cells do receive stronger PP input than DGCs at baseline (Fig. 4G). *Cdkl5*^{-/-} mice showed greater eEPSC amplitude in MOPP cells, but lower amplitude in DGCs, than did *Cdkl5*^{+/-} controls (Fig. 4G). Within-genotype analysis indicated a significant cell type effect in both *Cdkl5*^{+/-} (cell type, $F_{(1,56)} = 30.15$, $p < 0.001$; cell type \times stimulus intensity interaction, $F_{(20,1120)} = 12.43$, $p < 0.001$) and *Cdkl5*^{-/-} mice (cell type, $F_{(1,56)} = 106.26$, $p < 0.001$; cell type \times stimulus intensity

interaction, $F_{(20,1120)} = 61.90$, $p < 0.001$). Within-cell type analysis revealed a significant CDKL5 effect in both MOPP cells (genotype, $F_{(1,56)} = 7.39$, $p = 0.0090$; genotype \times stimulus intensity interaction, $F_{(20,1120)} = 3.07$, $p < 0.001$) and DGCs (genotype, $F_{(1,56)} = 20.21$, $p < 0.001$; genotype \times stimulus intensity interaction, $F_{(20,1120)} = 12.86$, $p < 0.001$). These data suggest that loss of CDKL5 amplifies the difference between MOPP cells and DGCs in excitatory synaptic transmission from the PP.

Because changes in synaptic transmission could arise on either the presynaptic or postsynaptic side, we next tested paired-pulse facilitation, which is inversely related to presynaptic neurotransmitter release, using the same dual patch settings. There was a significant interaction of the PPR between genotype and cell type (two-way ANOVA: $F_{(1,96)} = 5.05$, $p = 0.0270$) (Fig. 4H,I). Tukey's *post hoc* analysis revealed that *Cdkl5*^{-/-} mice had a greater PPR of DGCs than did *Cdkl5*^{+/-} controls (*Cdkl5*^{-/-} DGC 1.64 ± 0.12 vs *Cdkl5*^{+/-} DGC 1.31 ± 0.08 , $p = 0.0160$), indicating that CDKL5 loss decreased glutamate release from the PP onto these cells. Notably, the PPR in DGCs was higher than in MOPP cells in *Cdkl5*^{-/-} mice (*Cdkl5*^{-/-} MOPP 1.31 ± 0.08 vs *Cdkl5*^{-/-} DGC 1.64 ± 0.12 , $p = 0.0130$), whereas *Cdkl5*^{+/-} littermates sho-

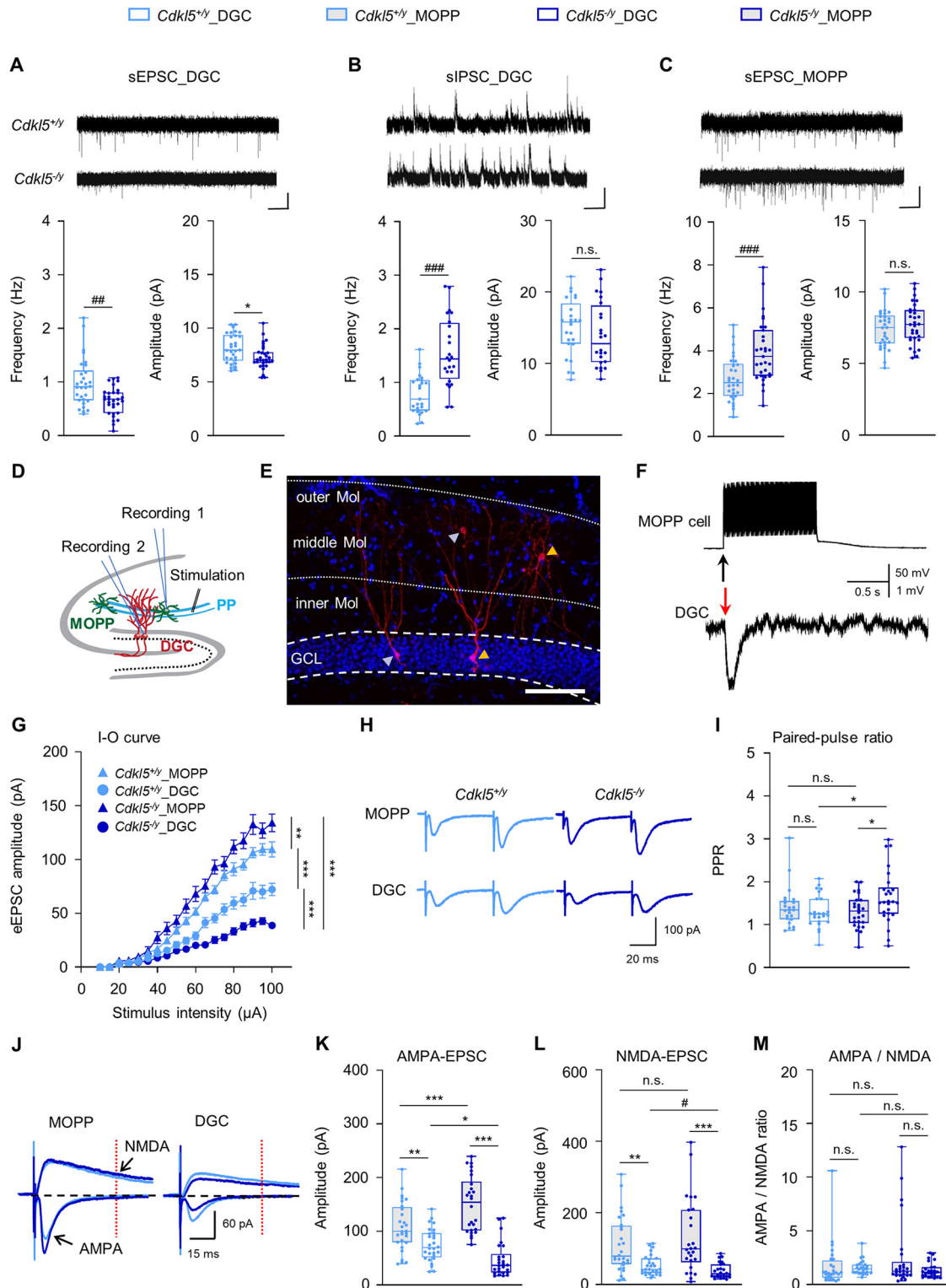


Figure 4. Male *Cdkl5*^{-/-} mice have impaired synaptic transmission in the PP to the DG. **A**, Top, Representative sEPSC traces recorded from the DGCs in *Cdkl5*^{-/-} mice and *Cdkl5*^{+/-} littermates. Calibration: 1 s, 10 pA. Bottom, Frequency and amplitude of sEPSCs measured from the DGCs in *Cdkl5*^{-/-} mice ($n_{\text{cells/animals}} = 31/5$) and *Cdkl5*^{+/-} littermates ($n_{\text{cells/animals}} = 30/5$). **B**, Top, Representative sIPSC traces of DGCs in *Cdkl5*^{-/-} mice and *Cdkl5*^{+/-} littermates. Calibration: 1 s, 15 pA. Bottom, Frequency and amplitude of sIPSCs measured from DGCs in *Cdkl5*^{-/-} mice ($n_{\text{cells/animals}} = 24/3$) and *Cdkl5*^{+/-} littermates ($n_{\text{cells/animals}} = 25/3$). **C**, Top, Representative sEPSC traces of MOPP cells in *Cdkl5*^{-/-} mice and *Cdkl5*^{+/-} littermates. Calibration: 1 s, 5 pA. Bottom, Frequency and amplitude of sEPSCs measured from MOPP cells in *Cdkl5*^{-/-} mice ($n_{\text{cells/animals}} = 31/5$) and *Cdkl5*^{+/-} littermates ($n_{\text{cells/animals}} = 30/5$). **D**, Schematic diagram of dual whole-cell recording configuration in MOPP cells (Recording 1) and DGCs (Recording 2). The evoked responses to the same stimulation were measured in pairs. **E**, Immunofluorescent image of dual-patched, biocytin-filled MOPP cells and DGCs in the dentate molecular layer and dentate granule cell layer, respectively. White and yellow arrowheads indicate the paired recorded cells. Mol, Molecular layer; GCL, granule cell layer. Scale bar, 100 μm. **F**, Representative recording traces of dual patch, physiologically demonstrating the direct connection from a MOPP cell to a DGC. Excitation of MOPP cell by current injection (3 nA, 100 Hz for 1 s) evoked an IPSP in the DGC. Black arrow indicates the beginning of activation train. Red arrow indicates the IPSP initiation with ~10 ms latency in the DGC. **G**, Pairwise analysis of eEPSC amplitude versus stimulus intensity in MOPP cells and DGCs of both *Cdkl5*^{-/-} and *Cdkl5*^{+/-} mice ($n_{\text{cells/animals}} = 29$ pairs/5 for each group). **H**, Representative traces of paired-pulse evoked responses with 50 ms interval recorded in MOPP cells and DGCs of *Cdkl5*^{+/-} and *Cdkl5*^{-/-} mice. **I**, Pairwise analysis of PPR in

wed no cell type difference ($Cdkl5^{+/y}$ MOPP 1.41 ± 0.10 vs $Cdkl5^{+/y}$ DGC 1.31 ± 0.08 , $p = 0.4910$). CDKL5 did not affect PPR in MOPP cells ($Cdkl5^{-/y}$ MOPP 1.31 ± 0.08 vs $Cdkl5^{+/y}$ MOPP 1.41 ± 0.10 , $p = 0.4680$), which is further confirmed by the unchanged RRP size and presynaptic release probability in MOPP cells of $Cdkl5^{-/y}$ mice (Extended Data Fig. 4-1), indicating that CDKL5 is not involved in the presynaptic release in MOPP cells. This suggests that there was less excitatory neurotransmitter release from the PP to the DGCs than to the MOPP cells in $Cdkl5^{-/y}$ mice, which is consistent with the data in Figure 4G.

A change in sEPSC amplitude is routinely attributed to a postsynaptic alteration in receptor function, number, or both. A change in sEPSC frequency could be because of either an altered probability of neurotransmitter release that was not detected using the paired-pulse analysis or a postsynaptic change in the number of functional AMPARs at synapses that were previously electrophysiologically “silent” (Isaac et al., 1995). Because CDKL5 loss increased MOPP cell sEPSC frequency but did not change the PPR and presynaptic release probability, we tested postsynaptic glutamatergic receptor function and number by recording AMPAR- and NMDAR-dependent currents in both MOPP cells and DGCs (Fig. 4J) (Umehiya et al., 1999; Etherton et al., 2011). Two-way ANOVA followed by Tukey’s *post hoc* analysis revealed the significant main effects of AMPAR-mediated current (AMPA-EPSC; genotype, $F_{(1,104)} = 0.75$, $p = 0.3890$; cell type, $F_{(1,104)} = 76.90$, $p < 0.001$; genotype \times cell type, $F_{(1,104)} = 20.06$, $p < 0.001$) and NMDAR-mediated current (NMDA-EPSC; genotype, $F_{(1,104)} = 0.04$, $p = 0.8370$; cell type, $F_{(1,104)} = 34.73$, $p < 0.001$; genotype \times cell type, $F_{(1,104)} = 1.99$, $p = 0.1610$) (Fig. 4K,L). AMPA-EPSC and NMDA-EPSC in MOPP cells were both larger than in DGCs in both genotypes (AMPA-EPSC: $Cdkl5^{+/y}$ MOPP 108.34 ± 8.55 vs $Cdkl5^{+/y}$ DGC 74.83 ± 5.73 , $p = 0.0030$; $Cdkl5^{-/y}$ MOPP 150.09 ± 10.09 vs $Cdkl5^{-/y}$ DGC 46.61 ± 6.18 , $p < 0.001$; NMDA-EPSC: $Cdkl5^{+/y}$ MOPP 111.08 ± 14.72 vs $Cdkl5^{+/y}$ DGC 53.52 ± 5.20 , $p = 0.0020$; $Cdkl5^{-/y}$ MOPP 131.83 ± 20.27 vs $Cdkl5^{-/y}$ DGC 38.05 ± 4.15 , $p < 0.001$). CDKL5 loss increased AMPA-EPSC in MOPP cells ($Cdkl5^{-/y}$ MOPP 150.09 ± 10.09 vs $Cdkl5^{+/y}$ MOPP 108.34 ± 8.55 , $p < 0.001$) but decreased AMPA-EPSC ($Cdkl5^{-/y}$ DGC 46.61 ± 6.18 vs $Cdkl5^{+/y}$ DGC 74.83 ± 5.73 , $p = 0.012$) and NMDA-EPSC ($Cdkl5^{-/y}$ DGC 38.05 ± 4.15 vs $Cdkl5^{+/y}$ DGC 53.52 ± 5.20 , Mann–Whitney test, $U = 227.0$, $p = 0.018$) in DGCs of $Cdkl5^{-/y}$ mice, which suggests that CDKL5 is critical to the function of postsynaptic glutamatergic receptors in the DG. The AMPA/NMDA ratios did not differ between the two genotypes for either cell type ($Cdkl5^{+/y}$ MOPP 1.71 ± 0.38 ; $Cdkl5^{+/y}$ DGC 1.55 ± 0.12 ; $Cdkl5^{-/y}$ MOPP 2.53 ± 0.63 ; $Cdkl5^{-/y}$ DGC 1.32 ± 0.14 ; two-way ANOVA: genotype \times cell type

←

four groups ($Cdkl5^{+/y}$ -MOPP and $Cdkl5^{+/y}$ -DGC, $n_{\text{cells/animals}} = 24/5$ per group; $Cdkl5^{-/y}$ -MOPP and $Cdkl5^{-/y}$ -DGC, $n_{\text{cells/animals}} = 26/5$ per group). **J**, Representative traces of evoked AMPAR-mediated EPSCs (negative going) recorded at -60 mV and compound EPSCs (positive going) recorded at 60 mV in MOPP cells and 40 mV in DGCs. Red dotted lines indicate 50 ms after stimulus, a time point at which the AMPAR-mediated contribution is considered negligible. **K–M**, Pairwise analysis of AMPAR- and NMDAR-mediated EPSCs in $Cdkl5^{-/y}$ mice ($n_{\text{cells/animals}} = 26$ pairs/4) and $Cdkl5^{+/y}$ littermates ($n_{\text{cells/animals}} = 28$ pairs/4). **K**, AMPAR-mediated component of EPSC. **L**, NMDAR-mediated component of EPSCs. **M**, AMPA/NMDA ratio. * $p < 0.05$, ** $p < 0.01$, *** $p < 0.001$; # $p < 0.05$, ## $p < 0.01$, ### $p < 0.001$, Mann–Whitney test. For details on presynaptic readily releasable size and release probability of MOPP cells as well as the intrinsic properties of DGCs and MOPP cells, see Extended Data Figures 4-1 and 4-2.

interaction, $F_{(1,104)} = 2.00$, $p = 0.161$; Fig. 4M). Together, these results suggest that, although CDKL5 loss did not alter the intrinsic properties of either MOPP cells or DGCs (Extended Data Fig. 4-2), it did alter the postsynaptic glutamatergic receptor functions in the PP to MOPP cells and DGCs.

Blocking GABAergic transmission in the DG enhances hippocampal memory in $Cdkl5^{-/y}$ mice

We next asked whether we could rescue the hippocampus-associated memory deficits in $Cdkl5^{-/y}$ mice by relieving this overinhibition in the DG circuitry. We intracranially infused the GABA_A receptor antagonist gabazine (1.0 ng per side) bilaterally into the DG of the dorsal hippocampus (Fig. 5A,D). The dose was selected based on previous publications (Chee et al., 2015; Lu et al., 2016) and a few pilot tests. We trained the mice with a fear conditioning task 13–15 min after infusing the gabazine or vehicle and tested for contextual and cued fear memory 24 h later. During the acquisition phase, both saline- and gabazine-injected $Cdkl5^{-/y}$ mice showed similar levels of exploratory behavior compared with $Cdkl5^{+/y}$ littermates before the foot shock ($Cdkl5^{-/y}$ -saline $4.36 \pm 1.55\%$ vs $Cdkl5^{+/y}$ -saline $2.40 \pm 0.27\%$, Mann–Whitney test, $U = 49.5$, $p = 0.1640$; $Cdkl5^{-/y}$ -gabazine $0.82 \pm 0.27\%$ vs $Cdkl5^{+/y}$ -gabazine $0.39 \pm 0.22\%$, Mann–Whitney test, $U = 42.0$, $p = 0.1850$). Immediately after the foot shock, saline-treated $Cdkl5^{-/y}$ mice froze less ($Cdkl5^{-/y}$ -saline $36.33 \pm 4.49\%$ vs $Cdkl5^{+/y}$ -saline $56.72 \pm 4.10\%$, two-tailed unpaired t test, $t_{(22)} = 3.356$, $p = 0.0029$) while gabazine-treated $Cdkl5^{-/y}$ mice showed a level of freezing similar to $Cdkl5^{+/y}$ mice ($Cdkl5^{-/y}$ -gabazine $38.67 \pm 6.77\%$ vs $Cdkl5^{+/y}$ -gabazine $40.53 \pm 5.16\%$, two-tailed unpaired t test, $t_{(20)} = 0.219$, $p = 0.8290$) (Fig. 5A). Twenty-four hours after the training, saline-treated $Cdkl5^{-/y}$ mice froze less in the conditioning context than did their saline-treated $Cdkl5^{+/y}$ littermates, thereby replicating the contextual memory impairment in the $Cdkl5$ nulls. Gabazine treatment significantly increased the freezing time of $Cdkl5^{-/y}$ mice in the conditioning context but did not alter the contextual freezing level in WT mice compared with their saline-treated controls (two-way ANOVA followed by Tukey’s *post hoc* analysis: genotype, $F_{(1,41)} = 99.16$, $p < 0.001$; treatment, $F_{(1,41)} = 0.23$, $p = 0.638$; $Cdkl5^{-/y}$ saline $6.44 \pm 1.31\%$ vs $Cdkl5^{+/y}$ saline $51.65 \pm 5.90\%$, $p < 0.001$; $Cdkl5^{+/y}$ saline $51.65 \pm 5.90\%$ vs $Cdkl5^{+/y}$ gabazine $49.28 \pm 4.26\%$, $p = 0.6760$; $Cdkl5^{-/y}$ saline $6.44 \pm 1.31\%$ vs $Cdkl5^{-/y}$ gabazine $12.70 \pm 1.11\%$, two-tailed unpaired t test, $t_{(19)} = 3.622$, $p = 0.0017$; Fig. 5B). As expected, local hippocampal gabazine infusion did not affect hippocampus-independent cued fear memory in either $Cdkl5^{-/y}$ mice or their $Cdkl5^{+/y}$ littermates (two-way ANOVA: genotype, $F_{(1,41)} = 3.40$, $p = 0.0730$, treatment, $F_{(1,41)} = 0.004$, $p = 0.953$; $Cdkl5^{+/y}$ saline $21.30 \pm 4.10\%$; $Cdkl5^{+/y}$ gabazine $13.86 \pm 4.58\%$; $Cdkl5^{-/y}$ saline $6.40 \pm 2.77\%$; $Cdkl5^{-/y}$ gabazine $14.30 \pm 3.61\%$; Fig. 5C). That the effect of gabazine was exclusive to the $Cdkl5^{-/y}$ mice confirms the functional consequences of the excessive GABAergic inhibitory transmission to the DG.

Forniceal DBS improves fear memory in female $Cdkl5^{+/-}$ mice

We previously showed that forniceal DBS can rescue hippocampal memory in a Rett syndrome mouse model (Hao et al., 2015). We decided to test whether forniceal DBS might prove beneficial in this intellectual disability disorder model as well. We implanted $Cdkl5^{+/-}$ mice and WT female littermates at 4.5 months with unilateral DBS electrodes to the fimbria-fornix. After recovery, both $Cdkl5^{+/-}$ mice and WT controls received 2 weeks of DBS or sham treatment 3 weeks

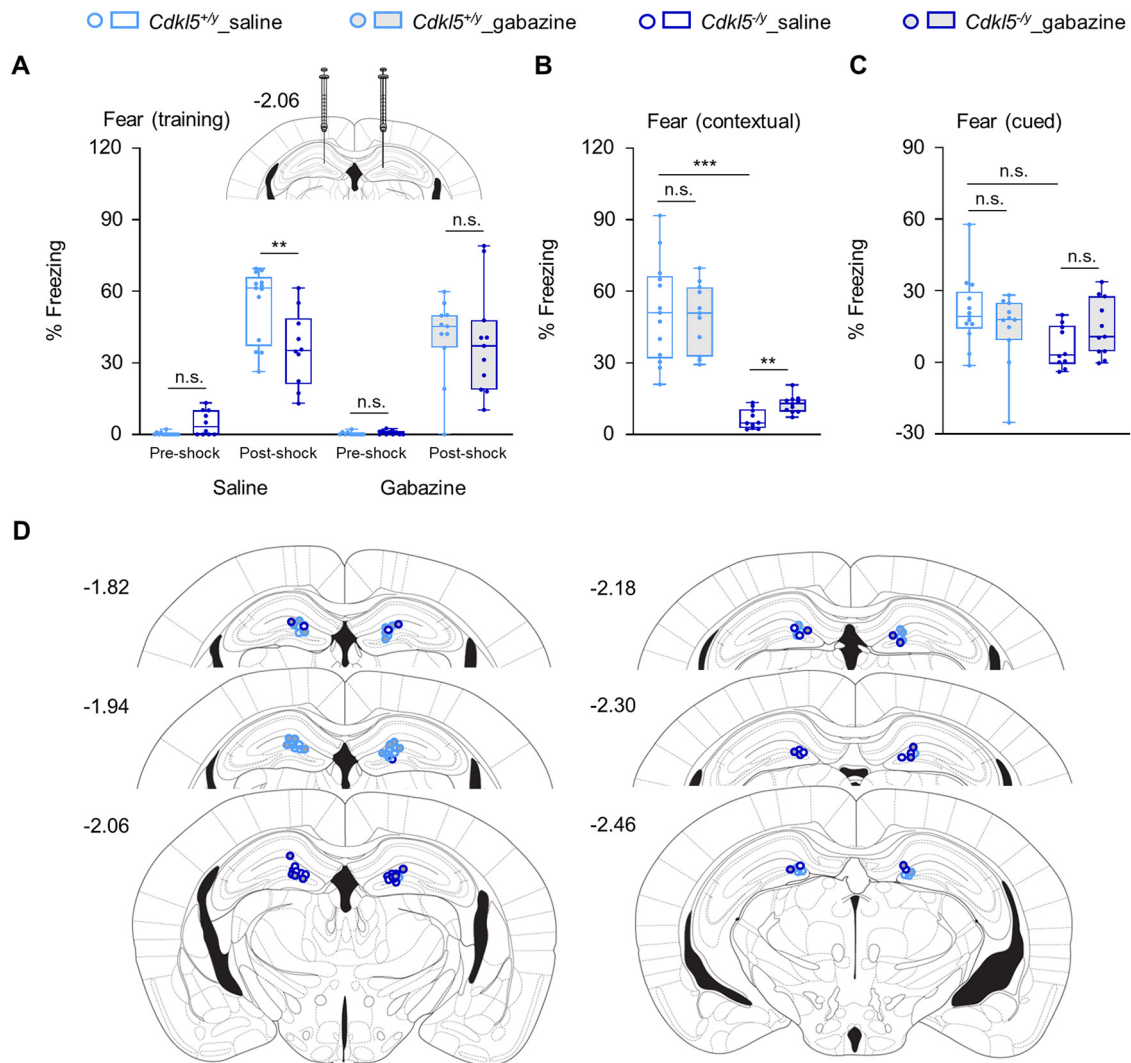


Figure 5. Blocking GABAergic transmission in the DG enhances hippocampal memory in $Cdkl5^{-/-}$ mice. **A**, During fear conditioning training, saline-treated $Cdkl5^{-/-}$ mice ($n = 10$) versus saline-treated $Cdkl5^{+/+}$ mice ($n = 13$) as well as gabazine-treated $Cdkl5^{-/-}$ mice ($n = 11$) versus gabazine-treated $Cdkl5^{+/+}$ mice ($n = 11$) showed comparable exploration levels before the first foot shock. Saline-treated $Cdkl5^{-/-}$ mice froze less than saline-treated $Cdkl5^{+/+}$ mice immediately after the second foot shock, whereas gabazine-treated $Cdkl5^{-/-}$ mice showed a similar level of freezing as gabazine-treated $Cdkl5^{+/+}$ mice after the foot shock. Inset, Diagram showing the placement of bilateral microinjection of gabazine or saline into the DG of dorsal hippocampi. The numbers on the upper left represent the posterior coordinate from the bregma. **B**, Contextual freezing responses of the fear memory 24 h after training. **C**, Cued freezing responses of the fear memory 24 h after training. **D**, Schematic representation of the dorsal hippocampi at six rostral-caudal planes for the microinjection sites of gabazine or saline in $Cdkl5^{-/-}$ mice and $Cdkl5^{+/+}$ littermates. The numbers on the left represent the posterior coordinate from the bregma. $**p < 0.01$, $***p < 0.001$.

before the fear conditioning task. During the acquisition phase, both sham- and DBS-treated $Cdkl5^{+/-}$ mice showed similar levels of exploratory behavior before the foot shock ($Cdkl5^{+/-}$ -sham $0.55 \pm 0.26\%$ vs $Cdkl5^{+/+}$ -sham $0.99 \pm 0.27\%$, Mann–Whitney test, $U = 104.5$, $p = 0.0790$; $Cdkl5^{+/-}$ -DBS $1.56 \pm 0.54\%$ vs $Cdkl5^{+/+}$ -DBS $0.86 \pm 0.25\%$, Mann–Whitney test, $U = 99.0$, $p = 0.4020$) and comparable freezing immediately after the foot shock ($Cdkl5^{+/-}$ -sham $15.94 \pm 3.39\%$ vs $Cdkl5^{+/+}$ -sham $19.17 \pm 4.15\%$, Mann–Whitney test, $U = 143.0$, $p = 0.7530$; $Cdkl5^{+/-}$ -DBS $21.76 \pm 4.74\%$ vs $Cdkl5^{+/+}$ -DBS $18.64 \pm 2.97\%$, two-tailed unpaired t test, $t_{(29)} = 0.548$, $p = 0.5880$) compared with $Cdkl5^{+/+}$ littermates (Fig. 6A). Twenty-four hours after the training, two-way ANOVA followed by Tukey's *post hoc* analysis revealed the significant effects of genotype ($F_{(1,61)} = 9.57$, $p = 0.003$) and genotype \times treatment interaction ($F_{(1,61)} = 8.51$, $p = 0.005$) on contextual memory. Sham-treated female $Cdkl5^{+/-}$ mice ($21.49 \pm 3.19\%$) replicated the contextual fear memory impairment compared with the $Cdkl5^{+/+}$ -sham group ($45.97 \pm 5.19\%$) ($p < 0.0010$). Forniceal

DBS rescued hippocampus-dependent contextual fear memory in $Cdkl5^{+/-}$ mice compared with sham-treated $Cdkl5^{+/-}$ mice ($Cdkl5^{+/-}$ sham $21.49 \pm 3.19\%$ vs $Cdkl5^{+/-}$ DBS $34.93 \pm 3.40\%$, $p = 0.0220$) (Fig. 6B). As a result, there is no difference between DBS-treated $Cdkl5^{+/-}$ mice ($34.93 \pm 3.40\%$) and sham-treated $Cdkl5^{+/+}$ animals ($45.97 \pm 5.19\%$) (two-tailed unpaired t test, $t_{(31)} = 1.756$, $p = 0.0890$). Notably, forniceal DBS also restored hippocampus-independent cued fear memory (two-way ANOVA followed by Tukey's *post hoc* analysis: genotype, $F_{(1,61)} = 5.53$, $p = 0.022$; treatment, $F_{(1,61)} = 9.14$, $p = 0.004$; $Cdkl5^{+/-}$ sham $24.78 \pm 5.28\%$ vs $Cdkl5^{+/+}$ sham $43.63 \pm 5.99\%$, $p = 0.0350$; $Cdkl5^{+/-}$ sham $24.78 \pm 5.28\%$ vs $Cdkl5^{+/-}$ DBS $47.86 \pm 8.41\%$, $p = 0.0120$; $Cdkl5^{+/-}$ DBS $47.86 \pm 8.41\%$ vs $Cdkl5^{+/+}$ sham $43.63 \pm 5.99\%$, Mann–Whitney test, $U = 129.0$, $p = 0.8150$; Fig. 6C). DBS did not alter contextual ($Cdkl5^{+/+}$ sham 45.97 ± 5.19 vs $Cdkl5^{+/+}$ DBS $35.65 \pm 4.10\%$, $p = 0.0810$) or cued ($Cdkl5^{+/+}$ sham $43.63 \pm 5.99\%$ vs $Cdkl5^{+/+}$ DBS $58.68 \pm 4.89\%$, $p = 0.0990$) fear memory in female WT mice,

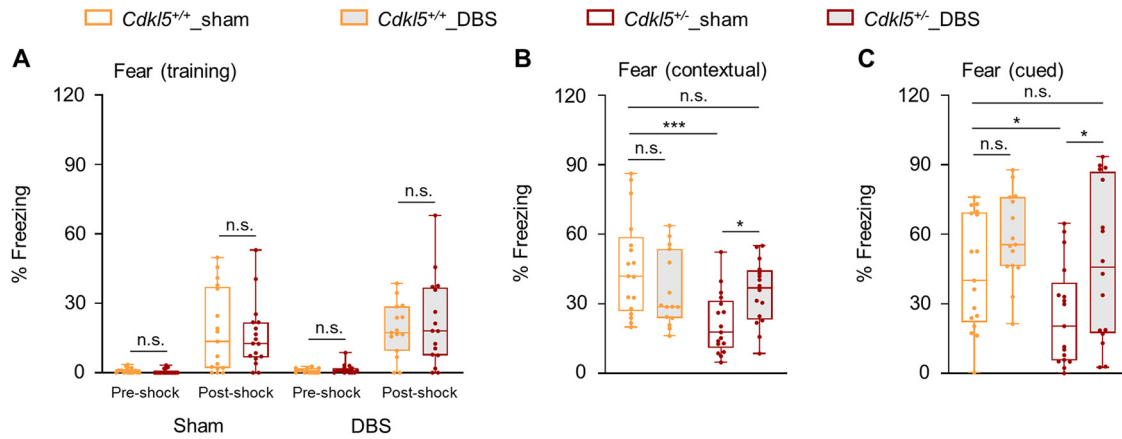


Figure 6. Fornical DBS improves fear memory in 6-month-old female *Cdkl5*^{+/-} mice. **A**, During fear conditioning training, sham-treated *Cdkl5*^{+/-} mice (*n* = 17) versus sham-treated *Cdkl5*^{+/+} mice (*n* = 17) as well as DBS-treated *Cdkl5*^{+/-} mice (*n* = 15) versus DBS-treated *Cdkl5*^{+/+} mice (*n* = 16) showed comparable exploration levels both before the first foot shock and froze at similar amount immediately after the second foot shock. **B**, Fornical DBS improved contextual fear memory in *Cdkl5*^{+/-} mice but not in WT littermates. **C**, Fornical DBS improved cued fear memory in *Cdkl5*^{+/-} mice but not in WT littermates. **p* < 0.05, ****p* < 0.001.

however, likely because of a ceiling effect of this model under these particular experimental conditions.

Forniceal DBS rescues hippocampal LTP and normalizes feedforward inhibition in the DG of freely moving *Cdkl5*^{+/-} mice

Given the DBS-induced benefits of memory, we next examined whether forniceal DBS improves hippocampal LTP in female heterozygous animals. Using similar procedures, we implanted *Cdkl5*^{+/-} mice and WT littermates at 4.5 months with unilateral DBS electrodes to the fimbria-fornix, stimulation electrodes to the PP, and ipsilateral recording electrodes in the DG (Hao et al., 2015). After recovery, we assigned both *Cdkl5*^{+/-} mice and WT controls to DBS or sham groups in which they received 2 weeks of DBS/sham treatment as in the fear memory experiment. Three weeks after the DBS/sham session, LTP induction potentiated population spikes for multiple days in all groups (one-way repeated-measures ANOVA, day 0, *p* < 0.001) (Fig. 7*A,B*). Two-way repeated-measures ANOVA revealed that LTP decreased in sham-treated *Cdkl5*^{+/-} mice compared with sham-treated *Cdkl5*^{+/+} group on day 0 ($F_{(1,12)} = 9.04, p = 0.011$) and day 1 ($F_{(1,12)} = 7.02, p = 0.021$), which replicated the LTP impairment in naive *Cdkl5*^{+/-} mice (Fig. 2*C*). Notably, forniceal DBS completely rescued LTP in *Cdkl5*^{+/-} mice (*Cdkl5*^{+/-}-DBS vs *Cdkl5*^{+/-}-sham; day 0, $F_{(1,12)} = 10.46, p = 0.007$; day 1, $F_{(1,12)} = 4.87, p = 0.048$; day 2, $F_{(1,12)} = 7.31, p = 0.019$) so that it equaled the LTP in sham-treated

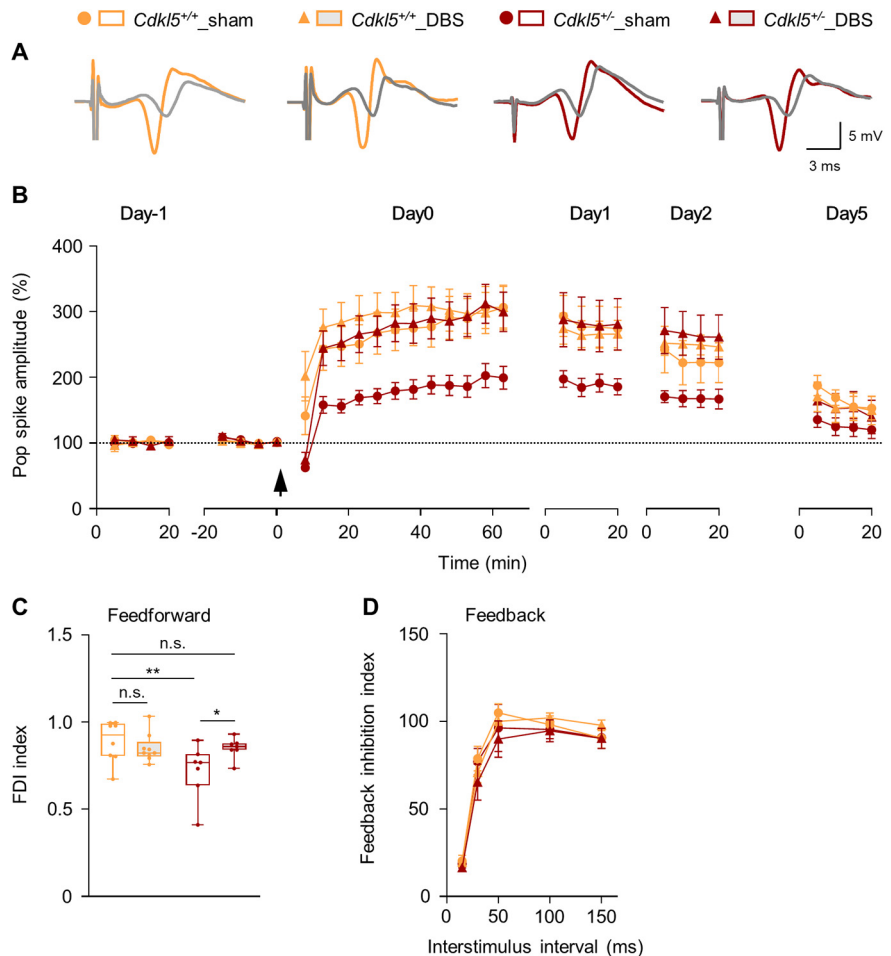


Figure 7. Forniceal DBS rescues hippocampal synaptic plasticity and local inhibitory circuit activity in the DG of freely moving *Cdkl5*^{+/-} mice. **A**, Superimposed traces of the PP recorded in the DG 5 min before (gray) and 55 min after tetani. **B**, Summary of *in vivo* LTP in *Cdkl5*^{+/+}-sham (*n* = 7), *Cdkl5*^{+/+}-DBS (*n* = 9), *Cdkl5*^{+/-}-sham (*n* = 7), and *Cdkl5*^{+/-}-DBS (*n* = 7) mice. LTP was induced by theta burst stimulation (arrow) on day 0 and followed up for 5 more days. **C**, Summary of FDI index in *Cdkl5*^{+/+}-sham (*n* = 8), *Cdkl5*^{+/+}-DBS (*n* = 9), *Cdkl5*^{+/-}-sham (*n* = 7), and *Cdkl5*^{+/-}-DBS (*n* = 7) mice. **D**, Summary of feedback inhibition index in *Cdkl5*^{+/+}-sham (*n* = 8), *Cdkl5*^{+/+}-DBS (*n* = 9), *Cdkl5*^{+/-}-sham (*n* = 7), and *Cdkl5*^{+/-}-DBS (*n* = 7) mice. **p* < 0.05, ***p* < 0.01.

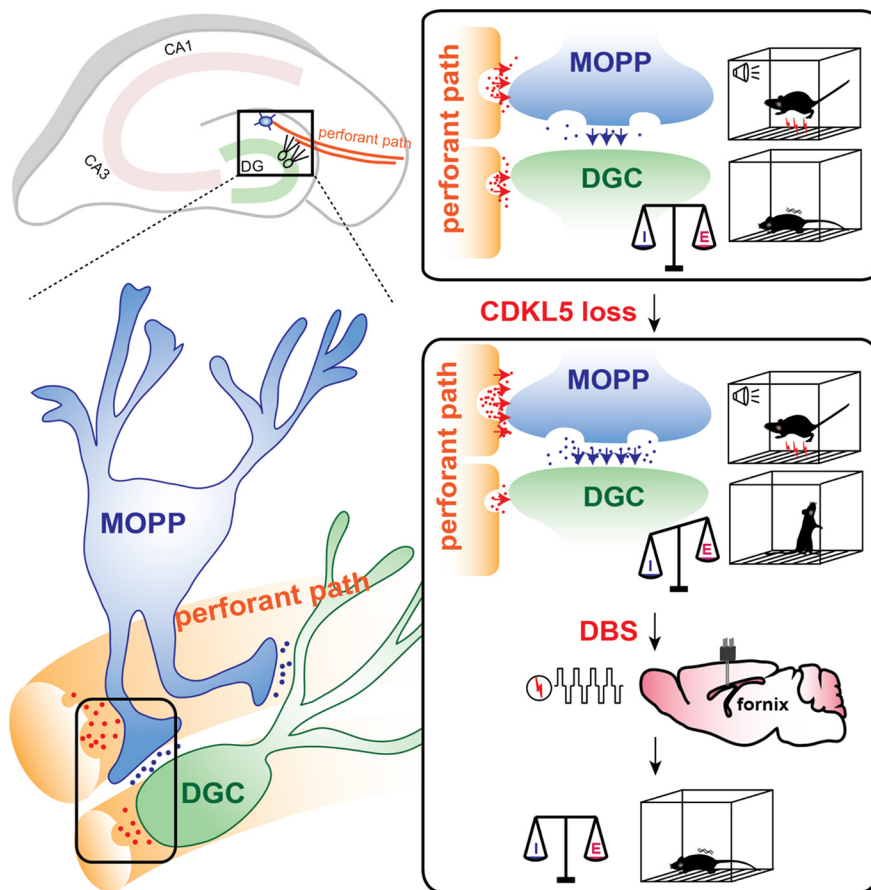


Figure 8. Fornical DBS rescues fear memory and hippocampal circuit activity in *Cdkl5* mutant mice. The PP originating in the entorhinal cortex innervates both MOPP cells and DGCs in the DG. The MOPP cells form synaptic connections with the DGCs and mediate feedforward inhibition of the perforant-to-DG pathway. In WT mice, the PP provides greater synaptic input to the MOPP cells than to the granule cells and maintains a balanced E/I in DGCs. Loss of CDKL5, however, further amplifies the difference in PP input between MOPP cells and DGCs: glutamate-mediated PP excitatory synaptic transmission increases to the MOPP cells but decreases to the DGCs cells in *Cdkl5* mutant mice. As a result, the stronger GABA-mediated inhibition from overactivated MOPP cells and decreased excitatory input directly from the PP shift the E/I of the granule cells to inhibition. This overinhibition of the DGCs contributes to hippocampal learning and memory deficits in *Cdkl5* mutant mice. Chronic fornical DBS rescues the feedforward inhibition of this pathway and the hippocampal memory in *Cdkl5*^{+/-} mice.

Cdkl5^{+/-} animals (*Cdkl5*^{+/-}-DBS vs *Cdkl5*^{+/-}-sham, $p > 0.05$ for all the test days). DBS did not alter LTP levels (*Cdkl5*^{+/-}-sham vs *Cdkl5*^{+/-}-DBS, $p > 0.05$ for all the test days) or hippocampal memory in WT animals, because of the same ceiling effect we observed before (Fig. 6B).

Last, we tested whether fornical DBS modulates feedforward and feedback inhibition in the DG in freely moving *Cdkl5*^{+/-} mice. We performed the same surgical preparations used for the LTP test. Three weeks after the 2-week DBS/sham treatment, we tested all 4 groups of mice for both feedforward and feedback inhibition (Fig. 3). For feedforward inhibition, two-way ANOVA revealed the significant main effects of genotype ($F_{(1,27)} = 4.60$, $p = 0.0410$) and genotype \times treatment interaction ($F_{(1,27)} = 4.68$, $p = 0.0400$) (Fig. 7C). Tukey's *post hoc* test indicated that sham-treated *Cdkl5*^{+/-} mice had lower FDI indices (indicating stronger feedforward inhibition) than sham-treated *Cdkl5*^{+/-} animals (*Cdkl5*^{+/-} sham 0.72 ± 0.06 vs *Cdkl5*^{+/-} sham 0.89 ± 0.04 , $p = 0.0060$). Fornical DBS restored the feedforward inhibition in *Cdkl5*^{+/-} mice (*Cdkl5*^{+/-} sham 0.72 ± 0.06 vs *Cdkl5*^{+/-} DBS 0.85 ± 0.02 , $p = 0.0320$; *Cdkl5*^{+/-} DBS 0.85 ± 0.02 vs *Cdkl5*^{+/-} sham 0.89 ± 0.04 , two-tailed unpaired *t* test, $t_{(13)} = 0.758$, $p = 0.4620$) without altering it in WT animals (*Cdkl5*^{+/-} sham

0.89 ± 0.04 vs *Cdkl5*^{+/-} DBS 0.85 ± 0.03 , $p = 0.4740$). Fornical DBS had no effect on feedback inhibition in either *Cdkl5*^{+/-} mice or WT littermates (two-way repeated-measures ANOVA: genotype, $F_{(3,27)} = 0.68$, $p = 0.5720$; genotype \times interval interaction, $F_{(12,108)} = 0.53$, $p = 0.8880$; Fig. 7D). These data show that fornical DBS rescues hippocampal LTP and normalizes feedforward inhibition in female *Cdkl5*^{+/-} mice.

Discussion

Hippocampus-dependent learning and memory deficits have been consistently demonstrated across CDD models (Wang et al., 2012; Fuchs et al., 2015; Okuda et al., 2018). Although several studies have addressed the molecular derangements involved (Fuchs et al., 2014; Trazzi et al., 2016; Okuda et al., 2017; Tang et al., 2019; Zhu and Xiong, 2019; Fuchs et al., 2020), the underlying neural circuit mechanisms of memory dysfunction have not been investigated. We therefore sought to understand how the molecular changes that follow CDKL5 loss affect physiology at the circuit, neuronal, and synaptic level. Our study highlights a novel circuit mechanism whereby loss of CDKL5 augments feedforward inhibition into the DG from overactivated MOPP cells, decreases excitatory activity from the PP, and suppresses the plasticity necessary for learning and memory formation. Remarkably, fornical DBS rescued hippocampal memory, synaptic plasticity, and feedforward inhibition in *Cdkl5* mutant mice (Fig. 8).

A few studies have examined CDKL5-mediated synaptic plasticity in different brain regions using brain slice preparations. CDKL5 loss in male nulls decreases LTP in the somatosensory cortex (Della Sala et al., 2016) and perirhinal cortex (Ren et al., 2019) but increases LTP in the Schaffer collateral to CA1 pathway of the hippocampus (Okuda et al., 2017). The CDKL5 knock-in mice also show increased early phase LTP and normal long-term depression in the Schaffer collateral to CA1 pathway (Yennawar et al., 2019). Interpretation of such *ex vivo* data, however, is complicated by mechanical damage to neural connections, changes in extracellular glutamate concentration, and alteration in immediate early gene expressions (Dolphin et al., 1982; French et al., 2001). Since the DG is crucial in gating contextual and spatial information from the entorhinal cortex to the hippocampus (Hargreaves et al., 2005) and in hippocampal memory (Sasaki et al., 2018), we examined LTP in the PP-DG pathway *in vivo*, which to our knowledge has never been studied in any CDD model. Loss of CDKL5 impairs LTP in this pathway in both male *Cdkl5* null and female *Cdkl5* heterozygous mice. Therefore, CDKL5 plays a role in regulating LTP in the DG and, by extension, hippocampal memory.

Impaired E/I balance is commonly found in mouse models of neurodevelopmental disorders and is thought to underlie a range of pathologies (Yizhar et al., 2011; Bateup et al., 2013; Han et al., 2013; Nelson and Valakh, 2015). Conditional KO of *CDKL5* in forebrain glutamatergic neurons increases both excitatory and inhibitory synaptic transmission in CA1 pyramidal neurons and induces hippocampal circuit hypoexcitability that is linked to the memory deficits (Tang et al., 2017). In contrast, *CDKL5* loss in the forebrain GABAergic neurons increases excitatory but not inhibitory transmission in CA1 pyramidal neurons and induces circuit hyperexcitability, contributing to autistic features (Tang et al., 2019). We found that *CDKL5* loss increased feedforward inhibition and reduced the E/I ratio in the DGCs. The E/I ratio difference between the projection neurons in DG and CA1 regions might stem from differences in the intrinsic properties of DGCs and CA1 pyramidal neurons or differences in overall network activity in the conventional KO model we used and the conditional KO of *CDKL5* in excitatory or inhibitory neurons. Although conditional KO models may provide valuable insight into the function of *CDKL5* in different types of neurons, our results showcase the collective hippocampal circuit defects that *CDKL5* loss causes and demonstrate that feedforward inhibition in the PP to DG contributes to memory deficits.

Of all the DG inhibitory interneurons, the function of the MOPP cells is least understood, partly because they were discovered only fairly recently (Amaral et al., 2007). We found that MOPP cells mediate the feedforward inhibition from the PP to the DGCs, which is consistent with a previous report (Li et al., 2013). Our observation that PP-initiated excitatory synaptic transmission is stronger in MOPP cells than in DGCs in WT mice indicates that the MOPP cell-mediated tonic feedforward inhibition helps enable normal circuit activity in the DG. We also found that *CDKL5* is vital to MOPP cell-mediated inhibition.

Previously, only impairments in the fear conditioning task had been reported in male nulls from the model used in this study (Wang et al., 2012). We show here that loss of *CDKL5* impaired hippocampal learning and memory in multiple tasks, in both male and female mutant mice. In particular, the clinically relevant female heterozygous mice have behavioral deficits comparable to those in the male nulls, although these deficits appear 2 months later because of mosaicism. These new findings are critical to understand the neurophysiological functions of *CDKL5* and validate the fact that female *Cdkl5*^{+/-} mice are a valuable model for testing therapeutic interventions.

This study also suggests that DBS's ability to rescue hippocampus-dependent learning and memory is not limited to particular molecular defects. We previously used DBS to rescue hippocampal circuit function and memory in a mouse model of Rett syndrome, which is caused by loss of function of MeCP2 (Hao et al., 2015), a protein whose function is completely unrelated to *CDKL5*. Consistent with our new finding showing that increased feedforward inhibition contributes to the behavioral deficits in *Cdkl5* mutant mice, DBS again rescued both memory deficits and hippocampal circuit dysfunction in parallel. Interestingly, fornical DBS also enhanced hippocampus-independent cued fear memory in *Cdkl5* heterozygous mice, something that we did not observe in Rett syndrome mice (Hao et al., 2015). We have yet to pinpoint why fornical DBS enhances cued fear memory. The amygdala and hippocampus act synergistically to form long-term memories of emotional events (Richter-Levin and Akirav, 2000; Phelps, 2004); it seems likely that either the amygdala-hippocampal

circuit itself, or the effect of DBS on the circuit, differs between *CDKL5*- and MeCP2-deficient mice. Further studies will be needed to decipher such differences.

It was proposed nearly a decade ago that interventions targeted at relevant neural circuits could correct the neural circuit defects in the CDD brain (Zoghbi and Bear, 2012). Our results validate this hypothesis and demonstrate that fornical DBS can relieve the feedforward inhibition in the PP and rescue hippocampus-dependent learning and memory deficits. Our results provide an important circuit-based understanding of *CDKL5*-mediated cognitive dysfunction. Fornical DBS may constitute a promising translational intervention for treating CDD and, possibly, other intellectual disability disorders.

References

- Allene C, Picardo MA, Becq H, Miyoshi G, Fishell G, Cossart R (2012) Dynamic changes in interneuron morphophysiological properties mark the maturation of hippocampal network activity. *J Neurosci* 32:6688–6698.
- Amaral DG, Scharfman HE, Lavenex P (2007) The dentate gyrus: fundamental neuroanatomical organization (dentate gyrus for dummies). *Prog Brain Res* 163:3–22.
- Andersen P, Holmqvist B, Voorhoeve PE (1966) Entorhinal activation of dentate granule cells. *Acta Physiol Scand* 66:448–460.
- Bateup HS, Johnson CA, Deneffrio CL, Saulnier JL, Kornacker K, Sabatini BL (2013) Excitatory/inhibitory synaptic imbalance leads to hippocampal hyperexcitability in mouse models of tuberous sclerosis. *Neuron* 78:510–522.
- Bouthour W, Megevan P, Donoghue J, Luscher C, Birbaumer N, Krack P (2019) Biomarkers for closed-loop deep brain stimulation in Parkinson disease and beyond. *Nat Rev Neurol* 15:343–352.
- Chee SS, Menard JL, Dringenberg HC (2015) The lateral septum as a regulator of hippocampal theta oscillations and defensive behavior in rats. *J Neurophysiol* 113:1831–1841.
- Corcoran KA, Maren S (2001) Hippocampal inactivation disrupts contextual retrieval of fear memory after extinction. *J Neurosci* 21:1720–1726.
- Della Sala G, Putignano E, Chelini G, Melani R, Calcagno E, Ratto GM, Amendola E, Gross CT, Giustetto M, Pizzorosso T (2016) Dendritic spine instability in a mouse model of *CDKL5* disorder is rescued by insulin-like growth factor 1. *Biol Psychiatry* 80:302–311.
- Dolphin AC, Errington ML, Bliss TV (1982) Long-term potentiation of the perforant path in vivo is associated with increased glutamate release. *Nature* 297:496–498.
- Etherton M, Foldy C, Sharma M, Tabuchi K, Liu X, Shamloo M, Malenka RC, Sudhof TC (2011) Autism-linked neuroligin-3 R451C mutation differentially alters hippocampal and cortical synaptic function. *Proc Natl Acad Sci USA* 108:13764–13769.
- Foss-Feig JH, Adkinson BD, Ji JL, Yang G, Srihari VH, McPartland JC, Krystal JH, Murray JD, Anticevic A (2017) Searching for cross-diagnostic convergence: neural mechanisms governing excitation and inhibition balance in schizophrenia and autism spectrum disorders. *Biol Psychiatry* 81:848–861.
- French PJ, O'Connor V, Jones MW, Davis S, Errington ML, Voss K, Truchet B, Wotjak C, Stean T, Doyere V, Maroun M, Laroche S, Bliss TV (2001) Subfield-specific immediate early gene expression associated with hippocampal long-term potentiation in vivo. *Eur J Neurosci* 13:968–976.
- Freund TF, Buzsáki G (1996) Interneurons of the hippocampus. *Hippocampus* 6:347–470.
- Fuchs C, Trazzi S, Torricella R, Viggiano R, De Franceschi M, Amendola E, Gross C, Calza L, Bartesaghi R, Ciani E (2014) Loss of *CDKL5* impairs survival and dendritic growth of newborn neurons by altering AKT/GSK-3beta signaling. *Neurobiol Dis* 70:53–68.
- Fuchs C, Rimondini R, Viggiano R, Trazzi S, De Franceschi M, Bartesaghi R, Ciani E (2015) Inhibition of GSK3beta rescues hippocampal development and learning in a mouse model of *CDKL5* disorder. *Neurobiol Dis* 82:298–310.
- Fuchs C, Gennaccaro L, Ren E, Galvani G, Trazzi S, Medici G, Loi M, Conway E, Devinsky O, Rimondini R, Ciani E (2020) Pharmacotherapy with sertraline rescues brain development and behavior in a mouse model of *CDKL5* deficiency disorder. *Neuropharmacology* 167:107746.

- Hainmueller T, Bartos M (2020) Dentate gyrus circuits for encoding, retrieval and discrimination of episodic memories. *Nat Rev Neurosci* 21:153–168.
- Han K, Holder JL Jr, Schaaf CP, Lu H, Chen H, Kang H, Tang J, Wu Z, Hao S, Cheung SW, Yu P, Sun H, Breman AM, Patel A, Lu HC, Zoghbi HY (2013) SHANK3 overexpression causes manic-like behaviour with unique pharmacogenetic properties. *Nature* 503:72–77.
- Hao S, Tang B, Wu Z, Ure K, Sun Y, Tao H, Gao Y, Patel AJ, Curry DJ, Samaco RC, Zoghbi HY, Tang J (2015) Forniceal deep brain stimulation rescues hippocampal memory in Rett syndrome mice. *Nature* 526:430–434.
- Hargreaves EL, Rao G, Lee I, Knierim JJ (2005) Major dissociation between medial and lateral entorhinal input to dorsal hippocampus. *Science* 308:1792–1794.
- Hsu TT, Lee CT, Tai MH, Lien CC (2016) Differential recruitment of dentate gyrus interneuron types by commissural versus perforant pathways. *Cereb Cortex* 26:2715–2727.
- Isaac JT, Nicoll RA, Malenka RC (1995) Evidence for silent synapses: implications for the expression of LTP. *Neuron* 15:427–434.
- Jones IW, Bolam JP, Wonnacott S (2001) Presynaptic localisation of the nicotinic acetylcholine receptor beta2 subunit immunoreactivity in rat nigrostriatal dopaminergic neurones. *J Comp Neurol* 439:235–247.
- Jones MW, Errington ML, French PJ, Fine A, Bliss TV, Garel S, Charnay P, Bozon B, Laroche S, Davis S (2001) A requirement for the immediate early gene *Zif268* in the expression of late LTP and long-term memories. *Nat Neurosci* 4:289–296.
- Kalscheuer VM, Tao J, Donnelly A, Hollway G, Schwinger E, Kubart S, Menzel C, Hoeltzenbein M, Tommerup N, Eyre H, Harbord M, Haan E, Sutherland GR, Ropers HH, Gecz J (2003) Disruption of the serine/threonine kinase 9 gene causes severe X-linked infantile spasms and mental retardation. *Am J Hum Genet* 72:1401–1411.
- Lee JW, Jung MW (2017) Separation or binding? Role of the dentate gyrus in hippocampal mnemonic processing. *Neurosci Biobehav Rev* 75:183–194.
- Leutgeb JK, Leutgeb S, Moser MB, Moser EI (2007) Pattern separation in the dentate gyrus and CA3 of the hippocampus. *Science* 315:961–966.
- Li Y, Stam FJ, Aimone JB, Goulding M, Callaway EM, Gage FH (2013) Molecular layer perforant path-associated cells contribute to feed-forward inhibition in the adult dentate gyrus. *Proc Natl Acad Sci USA* 110:9106–9111.
- Liu X, Ramirez S, Pang PT, Puryear CB, Govindarajan A, Deisseroth K, Tonegawa S (2012) Optogenetic stimulation of a hippocampal engram activates fear memory recall. *Nature* 484:381–385.
- Lozano AM, Lipsman N, Bergman H, Brown P, Chabardes S, Chang JW, Matthews K, McIntyre CC, Schlaepfer TE, Schulder M, Temel Y, Volkman J, Krauss JK (2019) Deep brain stimulation: current challenges and future directions. *Nat Rev Neurol* 15:148–160.
- Lu H, Ash RT, He L, Kee SE, Wang W, Yu D, Hao S, Meng X, Ure K, Ito-Ishida A, Tang B, Sun Y, Ji D, Tang J, Arenkiel BR, Smirnakis SM, Zoghbi HY (2016) Loss and gain of MeCP2 cause similar hippocampal circuit dysfunction that is rescued by deep brain stimulation in a Rett syndrome mouse model. *Neuron* 91:739–747.
- Malenka RC, Bear MF (2004) LTP and LTD: an embarrassment of riches. *Neuron* 44:5–21.
- Malleret G, Haditsch U, Genoux D, Jones MW, Bliss TV, Vanhoose AM, Weitlauf C, Kandel ER, Winder DG, Mansuy IM (2001) Inducible and reversible enhancement of learning, memory, and long-term potentiation by genetic inhibition of calcineurin. *Cell* 104:675–686.
- Maren S, De Oca B, Fanselow MS (1994) Sex differences in hippocampal long-term potentiation (LTP) and Pavlovian fear conditioning in rats: positive correlation between LTP and contextual learning. *Brain Res* 661:25–34.
- McHugh TJ, Jones MW, Quinn JJ, Balthasar N, Coppari R, Elmquist JK, Lowell BB, Fanselow MS, Wilson MA, Tonegawa S (2007) Dentate gyrus NMDA receptors mediate rapid pattern separation in the hippocampal network. *Science* 317:94–99.
- Morris RG, Garrud P, Rawlins JN, O'Keefe J (1982) Place navigation impaired in rats with hippocampal lesions. *Nature* 297:681–683.
- Moy SS, Nadler JJ, Young NB, Perez A, Holloway LP, Barbaro RP, Barbaro JR, Wilson LM, Threadgill DW, Lauder JM, Magnuson TR, Crawley JN (2007) Mouse behavioral tasks relevant to autism: phenotypes of 10 inbred strains. *Behav Brain Res* 176:4–20.
- Nakashiba T, Cushman JD, Pelkey KA, Renaudineau S, Buhl DL, McHugh TJ, Rodriguez Barrera V, Chittajallu R, Iwamoto KS, McBain CJ, Fanselow MS, Tonegawa S (2012) Young dentate granule cells mediate pattern separation, whereas old granule cells facilitate pattern completion. *Cell* 149:188–201.
- Nelson SB, Valakh V (2015) Excitatory/inhibitory balance and circuit homeostasis in autism spectrum disorders. *Neuron* 87:684–698.
- Okuda K, Kobayashi S, Fukaya M, Watanabe A, Murakami T, Hagiwara M, Sato T, Ueno H, Ogonuki N, Komano-Inoue S, Manabe H, Yamaguchi M, Ogura A, Asahara H, Sakagami H, Mizuguchi M, Manabe T, Tanaka T (2017) CDKL5 controls post-synaptic localization of GluN2B-containing NMDA receptors in the hippocampus and regulates seizure susceptibility. *Neurobiol Dis* 106:158–170.
- Okuda K, Takao K, Watanabe A, Miyakawa T, Mizuguchi M, Tanaka T (2018) Comprehensive behavioral analysis of the *Cdkl5* knockout mice revealed significant enhancement in anxiety- and fear-related behaviors and impairment in both acquisition and long-term retention of spatial reference memory. *PLoS One* 13:e0196587.
- Paxinos G, Franklin KB (2001) The mouse brain in stereotaxic coordinates. San Diego: Academic.
- Phelps EA (2004) Human emotion and memory: interactions of the amygdala and hippocampal complex. *Curr Opin Neurobiol* 14:198–202.
- Ren E, Roncace V, Trazzi S, Fuchs C, Medici G, Gennaccaro L, Loi M, Galvani G, Ye K, Rimondini R, Aicardi G, Ciani E (2019) Functional and structural impairments in the perirhinal cortex of a mouse model of CDKL5 deficiency disorder are rescued by a Trkb agonist. *Front Cell Neurosci* 13:169.
- Richter-Levin G, Akirav I (2000) Amygdala-hippocampus dynamic interaction in relation to memory. *Mol Neurobiol* 22:11–20.
- Rosenblum K, Maroun M, Richter-Levin G (1999) Frequency-dependent inhibition in the dentate gyrus is attenuated by the NMDA receptor blocker MK-801 at doses that do not yet affect long-term potentiation. *Hippocampus* 9:491–494.
- Samaco RC, McGraw CM, Ward CS, Sun Y, Neul JL, Zoghbi HY (2013) Female *Mecp2* (+/-) mice display robust behavioral deficits on two different genetic backgrounds providing a framework for pre-clinical studies. *Hum Mol Genet* 22:96–109.
- Sasaki T, Piatti VC, Hwaun E, Ahmadi S, Lisman JE, Leutgeb S, Leutgeb JK (2018) Dentate network activity is necessary for spatial working memory by supporting CA3 sharp-wave ripple generation and prospective firing of CA3 neurons. *Nat Neurosci* 21:258–269.
- Schneggenburger R, Meyer AC, Neher E (1999) Released fraction and total size of a pool of immediately available transmitter quanta at a calyx synapse. *Neuron* 23:399–409.
- Sloviter RS (1991) Feedforward and feedback inhibition of hippocampal principal cell activity evoked by perforant path stimulation: GABA-mediated mechanisms that regulate excitability in vivo. *Hippocampus* 1:31–40.
- Tang J, Dani JA (2009) Dopamine enables in vivo synaptic plasticity associated with the addictive drug nicotine. *Neuron* 63:673–682.
- Tang S, Wang JJ, Yue C, Takano H, Terzic B, Pance K, Lee JY, Cui Y, Coulter DA, Zhou Z (2017) Loss of CDKL5 in glutamatergic neurons disrupts hippocampal microcircuitry and leads to memory impairment in mice. *J Neurosci* 37:7420–7437.
- Tang S, Terzic B, Wang JJ, Sarmiento N, Sizov K, Cui Y, Takano H, Marsh ED, Zhou Z, Coulter DA (2019) Altered NMDAR signaling underlies autistic-like features in mouse models of CDKL5 deficiency disorder. *Nat Commun* 10:2655.
- Trazzi S, Fuchs C, Viggiano R, De Franceschi M, Valli E, Jedynak P, Hansen FK, Perini G, Rimondini R, Kurz T, Bartesaghi R, Ciani E (2016) HDAC4: a key factor underlying brain developmental alterations in CDKL5 disorder. *Hum Mol Genet* 25:3887–3907.
- Umeyama M, Senda M, Murphy TH (1999) Behaviour of NMDA and AMPA receptor-mediated miniature EPSCs at rat cortical neuron synapses identified by calcium imaging. *J Physiol* 521:113–122.
- Wang IT, Allen M, Goffin D, Zhu X, Fairless AH, Brodtkin ES, Siegel SJ, Marsh ED, Blendy JA, Zhou Z (2012) Loss of CDKL5 disrupts kinome

- profile and event-related potentials leading to autistic-like phenotypes in mice. *Proc Natl Acad Sci USA* 109:21516–21521.
- Wang Q, Mergia E, Koesling D, Mittmann T (2017a) Nitric oxide/cGMP signaling via guanylyl cyclase isoform 1 modulates glutamate and GABA release in somatosensory cortex of mice. *Neuroscience* 360:180–189.
- Wang Q, Yin P, Yu B, Zhao Z, Richter-Levin G, Yu L, Cao X (2017b) Down-regulation of dorsal striatal alphaCaMKII causes striatum-related cognitive and synaptic disorders. *Exp Neurol* 298:112–121.
- Weaving LS, Christodoulou J, Williamson SL, Friend KL, McKenzie OL, Archer H, Evans J, Clarke A, Pelka GJ, Tam PP, Watson C, Lahooti H, Ellaway CJ, Bennetts B, Leonard H, Gecz J (2004) Mutations of CDKL5 cause a severe neurodevelopmental disorder with infantile spasms and mental retardation. *Am J Hum Genet* 75:1079–1093.
- Whitlock JR, Heynen AJ, Shuler MG, Bear MF (2006) Learning induces long-term potentiation in the hippocampus. *Science* 313:1093–1097.
- Yennawar M, White RS, Jensen FE (2019) AMPA receptor dysregulation and therapeutic interventions in a mouse model of CDKL5 deficiency disorder. *J Neurosci* 39:4814–4828.
- Yizhar O, Fenno LE, Prigge M, Schneider F, Davidson TJ, O'Shea DJ, Sohal VS, Goshen I, Finkelstein J, Paz JT, Stehfest K, Fudim R, Ramakrishnan C, Huguenard JR, Hegemann P, Deisseroth K (2011) Neocortical excitation/inhibition balance in information processing and social dysfunction. *Nature* 477:171–178.
- Zhang TA, Tang J, Pidoplichko VI, Dani JA (2010) Addictive nicotine alters local circuit inhibition during the induction of in vivo hippocampal synaptic potentiation. *J Neurosci* 30:6443–6453.
- Zhu YC, Xiong ZQ (2019) Molecular and synaptic bases of CDKL5 disorder. *Dev Neurobiol* 79:8–19.
- Zoghbi HY, Bear MF (2012) Synaptic dysfunction in neurodevelopmental disorders associated with autism and intellectual disabilities. *Cold Spring Harb Perspect Biol* 4:a009886.